Seasonal Variability of Circulation and Hydrography in Hood Canal, Washington: A Numerical Model Study

Mitsuhiro Kawase and Bohyun Bahng

School of Oceanography, University of Washington
Seattle WA 98195

1. Introduction

Hood Canal, Washington (Fig.1) is a side branch of Puget Sound, the southernmost fjord estuary on the glaciated coast of the Pacific North America (Strickland, 1983). Its geometry is typical of a fjord, with small width (average 3.5 kilometers) relative to its length (110 kilometers) and substantial depth (average 100m) compared with a typical mid-latitude estuary. It has a long entrance sill that crests at twenty-five kilometers into the Canal at a depth of fifty-five meters. The Canal has one side branch of its own, Dabob Bay; the terminal portion of the Canal, Lynch Cove, connects to the main stem at a right angle through a constriction at Sisters Point.

Deep waters of the southern Hood Canal have historically had low dissolved oxygen concentration (ref.); in recent years, severity of the hypoxia has intensified to a point where negative effects on biota have become noticeable even to lay observers, and local communities have become concerned (ref.). In response, Hood Canal Dissolved Oxygen Program (HCDOP) has been initiated with federal funding support and participation of federal, state, tribal and local agencies and academic institutions.

In a typical calendar year, the basin starts in a relatively well-oxygenated state; then through the growth season a hypoxic layer develops near the bottom and towards the terminal end of the basin. In late summer to early fall, this hypoxic layer is seen to be lifted up to a position just below the surface pycnocline. A relatively small disturbance, such as a wind event, could bring this layer up to the surface and cause extensive fish kills along the shores of the southern Hood Canal (ref.). Such an event was observed in September 2006, and again in September 2010.

The above-described seasonal evolution of the hypoxia suggests that both physical and biogeochemical variability plays a role in its dynamics. Thus, a model that is capable of representing both the physical and the biogeochemical dynamics of a fjord estuary will be necessary. As a part of the HCDOP Integrated Assessment and Modeling, a three-dimensional, numerical hydrodynamic model has been developed for study of the exchange circulation in Hood Canal and as a basis for a comprehensive oxygen dynamics model of the Canal (Bahng et al., 2007). In this paper, we study the variability of exchange circulation over seasonal time scales and factors contributing to the variability.

2. Methods

2.1 Model selection

The Regional Ocean Modeling System (ROMS) of Haidvogel et al. (2008) is used for this study. ROMS is a three-dimensional, hydrostatic ocean circulation model with a bathymetry-following coordinate system and is widely used in regional, coastal and estuarine applications. Given initial and boundary conditions, the model predicts three components of velocity, sea surface height, and salinity. Because stratification in Hood Canal is dominated by fresh water / marine water contrast and because we

did not have adequate heat flux data at the sea surface, temperature was not used as a prognostic variable; it was set equal to ten degrees (approximately the annual average value) throughout the model run. Turbulent kinetic energy density and turbulence master length scale were determined using the Generic Length Scale parameterization of Umlauf and Burchard (2003) with parameters set to k-epsilon formulation; they were in turn used for specifying vertical eddy diffusivity and viscosity.

2.2 Grid

A fitted curvilinear coordinate system was used in the horizontal plane to represent the Hood Canal basin, with a minimum grid spacing of 160m, maximum of 440m and average of 255m (Figure 2). A stretched, bathymetry-following coordinate of Song and Haidvogel (S-coordinate) was used in the vertical with refined grid spacing near the surface and the bottom. The grid spacing ranged from 0.4m to 1.8m in the bottom and the surface layers; and to 5.4m in mid-water column. A total of fifty vertical layers were used. Basin depths were taken from the Puget Sound Digital Elevation Model (PSDEM 2000) of Finlayson et al. (2000). Points shallower than 10m were omitted; this excludes some small areas as Port Gamble, ends of Lynch Cove and Dabob Bay, and part of the Skokomish River delta (Figure 2).

2.3 Boundary conditions

A tidal elevation boundary condition was applied at the open boundary using published tidal constants for six constituents M2, S2, N2, K1, O1, P1 at Foulweather Bluff (see Fig. 1 for location), with slight adjustments to improve accuracy of tidal prediction. These were the same constituents used by Lavelle et al. (1988) in their pioneering channel model of Puget Sound tides except the overtide M4. A salinity boundary condition for the years 2005 – 2006 was developed using profiles from a long-term monitoring station ADM001 maintained by the Washington State and, starting in November 2005, the Hansville ORCA buoy located at the mouth of Hood Canal (Figure 3 top). Salinity values were applied using the asymmetric nudging technique of Marchesiello et al. (2001) with a nudging time scale of 4.8 hours during flood tide and twenty days during ebb tide.

At the bottom, a stress boundary condition with a quadratic bottom stress formulation

$$\vec{\tau}_{Bottom} = \rho_W C_D |\vec{u}_{Bottom}| \vec{u}_{Bottom} \quad (1)$$

was applied. A drag coefficient of 1.6×10^{-2} was used. The magnitude of the drag coefficient was adjusted until the modeled M2 phase difference between Foulweather Bluff and Union matched the value reported in Lavelle et al. (1988). Phase propagation of tidal oscillation is a measure of dissipation of tidal mechanical energy in the embayment (Freeland and Farmer, 1980), which supplies energy for mixing. This value is large compared with values used in previous models of the regional waters such as Lavelle et al. (1988; $2 \sim 6 \times 10^{-3}$) and Kawase and Thyng (2010; 3×10^{-3}), although Crean (1978) used a value as high as 3×10^{-2}. Also starting

in November 2005, a stress boundary condition was applied at the sea surface, with wind stress calculated from wind measurements at the ORCA buoys, and interpolated through the model domain (Figure 3 bottom). ORCA data gaps were filled with extrapolations from nearby weather stations such as at the Shelton air field based on regression from periods when both ORCA and weather station data were available.

2.4 Forcing

In addition to forcing through the boundary conditions, point source river discharges were applied at grid cells adjacent to river mouths (Figure 3 middle). River discharge data was collected as part of the HCDOP project and collated by Steinberg et al. (2010). This data set is monthly in time resolution, but it incorporates small streams and watersheds that are not part of the U.S. Geological Survey gauge network.

The model is started from a state of uniform salinity (29.3 PSU; the run becomes independent of the initial condition after approximately four months) on a nominal date of midnight February 2, 2005, and is run until midnight December 16, 2006. The one-year period of December 16, 2005 to the end of the run is designated as the verification period of the model. The start and the end of the period in the middle of the month is because of the monthly river flow data being assigned to the middle day of each month.

2.5 Diagnostics

Unfortunately, there were unavoidable disparities in sampling frequencies between data sets, different forcing and boundary conditions (and, in the case of the ORCA data, within the record). Because of this we cannot at this point perform a credible deterministic verification of the model (except tides) at timescales less than monthly. The study is instead directed towards simulation of the seasonal variability, which is resolved in all forcing data sets and which is of main interest to the problem of hypoxia. In order to focus on variability with intraseasonal and longer time scales, output variables as well as verification data were low-pass filtered using a fourth-order, forward and backward Butterworth filter with a cut-off period of ten days.

The modeled salinity and flow fields are sampled at a location off Hoodsport, WA near the southern end of the main channel, where one of the ORCA profiling buoys and an acoustic Doppler current meter (ADCP) were deployed for the period of verification. In addition, the model salinity was sampled and compared with ORCA data from a buoy that was deployed in Lynch Cove near Twanoh, WA. See Figure 1 for the sampling locations.

The exchange circulation is characterized in terms of transport streamfunction, which quantifies volumetric transport through the Canal. This is done in two different ways. First, a simple cross-channel ("Eulerian") integral is used to define the Eulerian overturning transport streamfunction Ψ. Let (x,y,z,t) be coordinates

along and across the channel, vertical (positive upward) and time, u(x,y,z,t) be along-channel velocity as a function of space and time, and h(x,y) be the water depth. Then

$$\Psi(x,z,t) = \int_y \int_{\min(z,-h)}^{z} u(x,y,z',t)dz'dy \quad (2)$$

The overturning transport streamfunction is a convenient way to depict vertical structure of a horizontally averaged circulation and is often used in the depiction of global thermohaline overturning. Second, a transport streamfunction can also be defined as a function of salinity in stead of depth as a vertical coordinate (MacCready, 2010): $\Psi_S(x, S, t)$ is volumetric transport of water whose salinity exceeds a certain value:

$$\Psi_S(x,S,t) = \iint_{S'>S} u(x,y,z,t)dA \quad (3)$$

where the areal integral is evaluated over the cross-sectional area where the salinity is greater than S. The latter is useful in more accurately quantifying the salt and freshwater transports in an estuary, and highlighting water mass transformations.

The former streamfunction is calculated throughout the Canal, while the latter is calculated at a cross-channel section south of Oak Head (see Figure 1) for comparison with previous transport estimates. This section is the nominal boundary between the southern and northern Hood Canal boxes in the box model of Babson et al. (2006) and is near Hazel Point, where Cokelet et al. (1990) previously obtained annual average transport estimates.

3 Results

3.1 Salinity and stratification

At the start of 2006, deep waters of Hood Canal were more saline than average (Figure 4); at surface a sharp halocline was capped by low salinity waters. Salinity of waters below the halocline decreased rapidly through the winter, and in mid-February the surface halocline started to weaken as well. In March the salinity of the deep waters started to increase gradually. The surface halocline was much weaker than in winter in this period, but was still present.

In mid-July the deep water salinity picked up its rate of increase, and it rose rapidly through the fall, especially during the second half of September. If we were to interpret the rising of the isohalines as indicative of the upwelling velocity, it would be remarkably fast: at its fastest the 30.4 PSU isohaline rose 56 meters per day, meaning that the entire water column would be replaced in less than two days at that speed.

Salinity in the middle and deep portions of the water column reached the maximum in late October – early November. The surface halocline was nearly absent in late summer and early fall, but began to be reestablished by the end of October. By the

end of the model run the water column returned to a state similar to the start of 2006, with high salinities at depth and a sharp halocline near the surface. Stratification is depicted in terms of Brunt-Väisälä frequency (Figure 5). Near-surface stratification (top panel) follows the coming and going of the fresh surface layer. In deeper waters (bottom panel), stratification is the highest during the period of decreasing salinity between January and April; and is the lowest during the strong upwelling period of summer – fall. The deep inflows that come in between July and September are initially practically unstratified. Overall, below thirty meters, stratification is quite weak throughout the year.

The seasonal variability of the water column salinity is consistent with a historical description of the seasonal cycle (Collias, et al., 1974). Comparison with the observed salinity profile at the Hoodsport ORCA (Figure 6; similarly low-passed, only depth levels where data is consistently available are plotted) shows that, in deep waters below the surface pycnocline, the model reproduces the overall character of the seasonal variability including high salnity near the start of the year: gradual decrease and descent of isohalines through winter and an abrupt increase of salinity and rising of isohalines in the fall. Even the pycnocline dip seen in depths down to 50m in February 2006 is simulated, although with less sharpness. A major difference, however, is the trend in the deep salinity in spring and summer: While the ORCA data show a gradual decrease through this period with the lowest values seen in July – August, the modeled salinity is the lowest in April with a gradual increase (except the very near bottom) through the period.

The model has a notable fresh bias in the deep waters throughout the year; the yearly average salinity between 11 and 50 m at the ORCA location is lower in the model than in the observations by 0.194 PSU, and below that, by 0.258 PSU (see Table 1). This is more clearly seen in the time series of average salinity below 50m (Figure 7, bottom). The largest discrepancy occurs in mid March, when it is as large as 0.8 PSU – while the model shows a rather abrupt decline in salinity in late winter followed by gradual increase until July, the observations show a much gentler decline that persists into summer. By the end of the summer the difference has narrowed, and the rapid increase in the fall towards high values of November – December is well simulated although a smaller fresh bias persists. One intriguing difference between the model and the observations is the apparent salt inversion in the deep waters observed in January 2006. This is because the deep water mass at this time was cold as well as saline (Figure 8), and temperature contributed significantly to the density of the water mass and thus to the stratification.

Nearer to the surface, the model's halocline appears too shallow; and overall the model has a salty bias this time (Figure 7, top; Table 1). The observed near-surface salinity is also much more variable, with the average salinity between 4 and 10m depth ranging by more than 5 PSUs as opposed to the modeled range of approximately 2.5 PSUs. It is possible that this variability is due to synoptic scale variability in river discharge, which is not resolved in the model forcing. Finally, the observations show strong near-surface warming in summertime (Figure 8). In

between, the mid-water column salinity (Figure 7, middle) is rather well simulated except the modeled salinity being too fresh at the start of the experimental period and the amplitude of the fresh event in February 2006 is too small.

Similar agreements and disagreements between the model and the data are found at the Twanoh ORCA location (Figures 9 and 10; Table 2). Here, the unrealistic disappearance of the surface halocline is particularly noticeable, especially between mid-May and November when the halocline is absent in the model while it is persistent in the ORCA data. The model appears to capture some of the significant intraseasonal variability, such as the fresh events in Februay and in mid-April to mid-May, albeit at greatly reduced amplitude. At depth, the model starts the verification period with salinity values too high, but in February the values become more realistic. While the model appears to miss the mid-May-to-July saline intrusion, in the latter half of the year it is more successful in reproducing observed salinity values, including the peak of the late Fall maximum. The model captures the overall seasonal variation of salinity at depth (Figure 10, bottom), especially in terms of the rate of its rising from a low in mid-February to the late Fall maximum.

Comparison of stratification at the Hoodsport ORCA (Figure 11) shows that, in the upper 40m, the model stratification is too weak, reflecting the halocline being too shallow and weak in the model. Below 40m the modeled stratification is close to the observed, except in the aftermath of the salt intrusion in the fall (Figure 11, rightmost panel) when the model is too stratified at depth.

3.2 Velocity and transport

Along-channel velocity at Hoodsport (Figure 12, positive is inflow into the Canal) shows a persistent outflow in the surface halocline that is particularly strong in winter. In January and November of 2006, this outflow is immediately compensated by an inflow whose core is also shallow, around 5m. Below this is another layer of outflow, whose core is around 30m in January and from 40 to 80m in November. In mid-February, the inflow layer shifts deeper and establishes its core around 30m. The inflow core stays at this depth until August, although there is a strong intraseasonal variability that from time to time reverses the flow. There is a deeper, highly variable outflow layer whose core depth starts around 70m and ranges from 40 to 85m; below this is a layer of inflow with a core depth of 95m. This latter is again highly variable.

In late September, this deepest inflow core momentarily strengthens greatly. This is coincident with the rapid rising of the isohalines (Figure 4), and evidently denotes the deep intrusion that lifts up existing deep water. This inflow core decays towards the end of the modeled period with an oscillation of roughly a monthly period. Overall, the along-channel flow in the deep layer is dominated by variability of monthly time scales.

For comparison, a similarly low-pass filtered along-channel velocity from an ADCP placed next to the Hoodsport ORCA buoy is plotted (Figure 13). Unfortunately the

ADCP cannot resolve the layers immediately adjacent to sea surface; and thus missed the outflowing surface layer. In contrast to the modeled field, observations show the layer between 5 and 10 meters to be dominantly inflowing; below this the currents are quite weak and again highly variable, but with a shorter time scale of variability than is seen in the model. The amplitude of the variability is also less in the observations than in the model.

In spite of the obvious discrepancies between the observed and the modeled currents, there are also features that are in common. Most significant is the deep intrusion in late September that triggers deep upwelling. The observed strength of the intrusion is somewhat weaker than in the model. The outflow that overlies this intrusion between 10 and 60 meters is also seen both in the observations and in the model. Finally, there is a shallow, event-like outflow in February both in the model and in the observations, with the model's timing slightly later than was observed.

Mean overturning streamfunction (Figure 14) over the period of model verification show a two-layer exchange circulation. The depth of no motion between the outgoing surface layer and the incoming deep layer is relatively deep, starting at 20m over the entrance sill and reaching 40m at the entrance to Dabob Bay 43 kilometers into the Canal. Past the underwater fan of the Hamma Hamma River (the bump on the bottom at 68km), it shallows considerably up to less than twenty meters, and in this shallow state the exchange circulation enters Lynch Cove (the shallow terminal basin beyond 90km). The streamfunction also indicates substantial refluxing (Cokelet and Stewart, 1985) of the outgoing surface layer just landward of the entrance sill. The exchange transport increases from 3012 m^3/s just seaward of the sill to 5851 m^3/s immediately landward; and stays above 4000m^3/s until past the Dabob Bay entrance.

As may be inferred from salinity and velocity changes (Figures 4 and 11), the exchange circulation varies significantly over the course of the year (Figure 15). The exchange is weaker and shallower than the average throughout the first eight months of the verification period, but deepens and strengthens in August, reflecting the onset of the fall intrusion bringing saline deep waters. Once the deep basin is filled with the new deep water, the exchange circulation retreats to the shallower position seen during most of the year. However, superimposed on this is considerable intraseasonal variability, most prominently at fortnightly timescales (Figure 16) reflecting modulation of mixing at the sill due to spring-neap and lunar declinational cycles. Exchange is at its strongest during neap tide, and weakest during spring tide (Geyer and Cannon, 1982); it also reaches deepest during neap tide and is shallowest during spring tide (Leonov and Kawase, 2008).

Salinity-averaged transport streamfunction Ψ_S is effective in showing the variation of exchange transport as well as what kind of water mass is coming into the Canal (Figure 17 top, plotted at the Oak Head section). The exchange is the strongest (over 9000 m^3/s) and the incoming water the most saline (30.5 PSU) at the start of the

verification period in December 2005; then both the transport and the salinity decrease to a minimum in mid-February. Thereon, the salinity of the incoming water increases slowly while the transport shows strong intraseasonal variability at fortnightly time scales described above. The rapid rise in salinity and transport magnitude in September indicates the Fall intrusion.

Comparison of exchange transport at Oak Head with previous works (Cokelet et al, 1990; Babson et al., 2006) shows that the exchange circulation in the model is much more vigorous than the previous estimates (Figure 17 bottom). The modeled annual average transport is 4980m^3/s, higher than the upper limit of Cokelet et al.'s estimate (3600m^3/s) as well as the annual average of the Babson et al. (2006) model (3526m^3/s). The possibility that the model may be overestimating the transport is consistent with other model-data discrepancies. The fresh bias in the deep waters (Figure 7) and the stratification deficiency (Figure 11) are indicative of excessive mixing in the model, which in turn would imply larger exchange transport from the Knudsen relation. The overall more vigorous circulation seen in Figure 12 is also consistent. On the other hand, the modeled exchange circulation shows much short horizontal-scale variability in this portion of the Canal (Figure 14) and the Oak Head section, as it happens, sits on top of a small recirculatory cell. Only six kilometers seaward (and closer to Hazel Point), the annual average transport decreases to a minimum of 3186m^3/s.

Apart from the magnitude difference in transport, the Babson et al. box model shows a much more gradual increase and an earlier peaking of the Fall intrusion. This is likely due to the smoothing inherent in the seasonal composite forcing of the box model, although interannual variability in the timing of the Fall intrusion may also be involved. Finally, the box model shows greatly diminished exchange outside the Fall intrusion, with the transport value falling below 1000m^3/s. There is no such drastic collapse happening in the model. This may be reflecting a limitation of the box model with a rigidly fixed level of no motion between the outgoing upper layer and the incoming lower layer. The level of no motion in the present model is variable over time (Figure 13); when the level does not match the fixed level, circulation collapse or even reversal may result in the box model. This was also seen in the exchange between the Main Basin of Puget Sound and Admiralty Inlet (Babson et al., 2006).

4 Discussion

4.1 Effects of temperature variability

As indicated in Section 2.1, temperature was not modeled actively because we did not have a complete set of forcing parameters needed for such modeling, including a complete suite of heat fluxes at the air-sea interface and temperature of the incoming river water. It is generally assumed that temperature effects are secondary to those of salinity contrasts and variability on the dynamics of the exchange circulation.

On the other hand, some of the discrepancies between the observed and modeled hydrography may be due to a lack of temperature effects on the model density, such as the persistent halocline in summer and observed deep salinity inversion in January 2006. Accordingly we ran the model with a variable temperature boundary condition at the open boundary, with values taken from ADM001 and Hansville ORCA as for the salinity boundary condition. No air-sea heat fluxes were imposed, and the river temperature was fixed at ten degrees centigrade. Incorporation of temperature does result in improvement in the modeled salinity, especially in the middle part of the water column (Figure 18). It hasn't eliminated the fresh bias in the model, but the increasing trend in the deep salinity in the spring and summer is no longer there, and the largest discrepancy in March is reduced to 0.5 PSU. It has not resulted in improvements in the near-surface salinity, but this may not be affected strongly by the deep temperature.

This improvement is evident in the model error statistics. While the bias error has slightly worsened (from -0.194 to -0.213 PSU for the 11 – 50m range; -0.258 to -0.272 PSU for the 51 – 96m range), the bias-corrected RMS error has decreased for both depth ranges, from 0.332 to 0.181 PSU and from 0.280 to 0.152 PSU respectively. Correspondingly, the relative error has decreased from 20.7% to 13%, and from 22.2% to 12.3% respectively.

This improvement may indicate that thermal forcing on the canal may play an important secondary role in its seasonal dynamics. It is also promising from a modeling point of view that incorporation of temperature results in an improved simulation. It would be desirable for future monitoring plans for the Canal to include measurements of a complete suite of parameters needed for air-sea flux estimates (air temperature, humidity, wind, short and long wave radiation) as well as river water temperature.

4.2 Factors contributing to the seasonal variability

Circulation and hydrography of Hood Canal show a clear and substantial seasonal cycle, and the model appears capable of capturing at least essential aspects of the physical variability. Understanding the cause of this variability will be important in assessing the Canal's sensitivity to natural and anthropogenic changes that might affect the hypoxia. Accordingly we ran a set of experiments, in which variability in one of the forcings – wind stress at the sea surface, river discharge, and salinity boundary condition at the open boundary – was eliminated and the forcing values set to period averages (in the case of wind stress, it was set to zero). The goal is to assess the importance of each of the forcing factors in affecting the canal's circulation.

It should be pointed out that these do not necessarily represent experiments in which wind, river variability and outside salinity variability are in turn completely eliminated. Both wind and river variability are likely implicit in the salinity variability at the Northern ORCA, so their effect may be indirectly felt through the open boundary condition. Also, all three factors are likely to co-vary under changes

in the climate regime. Strictly speaking, these experiments should be interpreted as exploring the model's sensitivity to different boundary conditions. Nevertheless we believe they can provide working hypotheses about factors influencing the circulation in Hood Canal.

The three experiments are compared with one another and with the full forcing experiment in terms of salinity at the Hoodsport ORCA location (Figure 19, equivalent of Figure 7) and Eulerian average transport at the Oak Head section (Figure 20, equivalent of Figure 17 bottom).

Eliminating wind stress (green lines) does little to the salinity values and the exchange transport. Holding the river discharge constant (blue lines) results in higher values of salinity from January to April and again at the end of the verification period. It also decreases the salinity in the top and the middle parts of the water column from July to November. These changes can be understood primarily in terms of the river discharge level relative to the mean (Figure 3 middle): the months in which the salinity value decreased (increased) are the months in which monthly river discharge was below (above) average. This decrease in river discharge from the monthly value results in significant decrease in the exchange circulation from January to April.

The largest changes are seen when the salinity values at the open boundary are held constant. In the deep layer (Figure 19 bottom), the seasonal cycle is almost completely eliminated; it is also much attenuated in the top and the middle layers, with lower values in months with high river discharge. The seasonal cycle of the exchange circulation is completely altered, with the highest exchange seen in winter months, not during the period of the observed saline intrusion which, actually, becomes a time of weakest exchange flow.

These results indicate that hydrographic conditions outside the mouth of the Canal may have a significant influence on the circulation and the hydrography of the Canal. Hood Canal is likely strongly affected by the conditions in the rest of Puget Sound, Salish Sea, and Pacific coastal waters; understanding its variability would require understanding the connection between the Canal and the larger body of water. They also underscore the importance of the boundary conditions forcing the model, but especially the condition at the open boundary. It is suggested that future monitoring plans for the Canal include continued monitoring of the inflow boundary condition at the Canal entrance, such as was provided by the Hansville ORCA buoy during the study period (considering the simplicity of the profiles there (ref.), however, it could be done with less vertical resolution). It would also be desirable for the present model to obtain boundary conditions from a larger, regional scale circulation model such as that of Sutherland et al. (2010), with the eventual goal being a two-way coupling such that the larger scale model can in turn incorporate information with the finer scale model of the Canal.

5. Summary

As a first attempt at modeling a complex body of water that is Hood Canal, this model has succeeded in capturing the essential seasonal dynamics. While there are many aspects of the model that need clear improvement, it is believed the issues are not fundamental (except as noted below), and can be addressed through further refinement of grid resolution, numerical techniques and parameterizations, and improvement of boundary conditions.

With regards to the purpose of HCDOP in understanding the hypoxia dynamics, the aspect of the model that requires the most improvement is near-surface stratification, especially disappearance of the halocline in summer. It would have a significant influence on the surface primary production (REF?), which would result in biological oxygen demand at depth. To address this issue, it would desirable to directly compare model-predicted turbulent eddy diffusivity with estimates from *in situ* turbulence measurements. Also, the present model does not include wetting and drying of tidal flats where much of the fresh water transformation is expected to take place; this could have an influence on the shaping of the near-surface stratification. This process is incorporated in newer versions of ROMS, and could be implemented into the model if accurate elevation data for the tidal flats are available. Finally, a terrain-following coordinate model such as ROMS (as well as many hydrodynamic models used in coastal applications), applied to a water body with steep bathymetry such as Hood Canal, would be significantly challenged to represent tight near-surface gradients accurately unless horizontal resolution is sufficient to resolve the gradient along a coordinate surface.

The model also underscores the importance of high quality boundary conditions. Ideally, the requisite boundary conditions – wind stress, heat and fresh water fluxes at the sea surface, river discharge rates and river water temperature, sea surface elevation, currents and tracer quantities such as temperature and salinity at the open boundary – are all available at a comparable time resolution; however, this is unlikely to be realized without possibly unrealistic level of resources committed to making observations.

Based on the performance of the model so far, the highest-priority new observation / improvement of the existing observations is that of the parameters related to heat flux at the sea surface. These include air temperature, humidity, wind speed, downward shortwave radiation and outgoing long wave radiation. *In situ* measurements are essential for wind and highly desirable for other meteorological parameters. Because the Canal sits in a shallow channel, local terrain effects are significant on the wind. Other parameters except long wave radiation are measured by a weather sensor mounted on each ORCA buoy, but reliability of these sensors has been a problem. Upgrading them would fill a needed data gap. Alternatively they may be obtained from a high-resolution regional weather model (such as the Weather Research and Forecasting Model now run routinely at four kilometer

resolution and experimentally at 1 1/3 kilometer resolution at the University of Washington Department of Atmospheric Sciences).

Acknowledgments

This work is supported by Hood Canal Dissolved Oxygen Program – Integrated Assessment and Modeling (HCDOP-IAM).

References

Babson, A.L., M. Kawase and P. MacCready, 2006, Seasonal and Interannual Variability in the Circulation of Puget Sound, Washington: A Box Model Study, Atmosphere-Ocean, 44, 29-45.

Bahng, B., M. Kawase, J. Newton, A. Devol and W. Ruef, 2007, Numerical Simulation of hypoxia in Hood Canal, USA, 2007 Georgia Basin Puget Sound Research Conference Proceedings.

Cokelet, E.D. and R.J. Stewart, 1985, The Exchange of Water in Fjords: The Efflux/Reflux Theory of Advective Reaches Separated by Mixing Zones, Journal Of Geophysical Research, 90, 7287-7306.

Cokelet, E.D., R.J. Steward and C.C. Ebbesmeyer, 1990, The annual mean transport in Puget Sound, NOAA Technical Memorandum ERL PMEL-92, 59pp.

Collias, E., N. McGary, and C.A. Barnes, 1974, Atlas of physical and chemical properties of Puget Sound and its approaches, Washington Sea Grant Publication WSG 74-1, Seattle, 235pp.

Crean, P.B., 1978, A numerical model o f barotropic mixed tides between Vancouver Island and the mainland and its relation to studies o f the estuarine circulation, in: Hydrodynamics of Estuaries and Fjords, ed by J.C. Nihoul, Elsevier, Amsterdam, pp. 283-313.

Finlayson, D.P., R.A. Haugerud, H. Greenberg, and M.G. Logsdon, 2000, Puget Sound Digital Elevation Model, University of Washington, http://ocean.washington.edu/data/pugetsound/psdem2000.html, accessed June 18, 2010.

Freeland, H. J., and Farmer, D. M., 1980, Circulation and energetics of a deep, strongly stratified inlet", Canadian Journal of Fisheries and Aquatic Sciences, 37, 1398-1410

Geyer, W.R., and G.A. Cannon, 1982, Sill processes related to deep water renewal in a fjord, Journal of Geophysical Research, 87(C10), 7985-7996.

Haidvogel, D.B., H. Arango, W.P. Budgell, B.D. Cornuelle, E. Curchitser, E. Di Lorenzo, K. Fennel, W.R. Geyer, A.J. Hermann, L. Lanerolle, J. Levin, J.C. McWilliams, A.J. Miller,

A.M. Moore, T.M. Powell, A.F. Shchepetkin, C.R. Sherwood, R.P. Signell, J.C. Warner, J. Wilkin, 2008, Ocean forecasting in terrain-following coordinates: Formulation and skill assessment of the Regional Ocean Modeling System, Journal of Computational Physics, 227, 3595-3624.

Kawase, M., and K.M. Thyng, 2010, Three-dimensional hydrodynamic modelling of inland marine waters of Washington State, United States, for tidal resource and environmental impact assessment, IET Renewable Power Generation, in press.

Lavelle, J.W., H.O. Mofjeld, E. Lempriere-Doggett, G.A. Cannon, D.J. Pashinski, E.D. Cokelet, L. Lytle and S. Gill, 1988, A multiple connected channel model of tides and tidal currents in Puget Sound, Washington and a comparison with updated observations, NOAA Technical Memorandum ERL PMEL-84.

Leonov, D., and M. Kawase, 2008, Sill dynamics and fjord deep water renewal: idealized modeling study, Continental Shelf Research, 29, 221–233.

MacCready, P., Calculating estuarine exchange flow using isohaline coordinates, submitted to Journal of Physical Oceanography.

Marchesiello, P., J.C. McWilliams, and A. Shchepetkin, 2001, Open boundary conditions for long-term integration of regional oceanic models, Ocean Modelling, 3, 1-20.

Song, Y.T. and D.B. Haidvogel, 1994, A semi-implicit ocean circulation model using a generalized topography-following coordinate system, Journal of Computational Physics, 115, 228-244.

Steinberg, P.D., M.T. Brett, J.S. Bechtold, J.E. Richey, L.M. Porensky, and S.N. Osborne, The Influence of Watershed Characteristics on Nitrogen Export to and Marine Fate in Hood Canal, Washington, USA, submitted to Biogeochemistry.

Strickland, R.M., 1983, The Fertile Fjord: Plankton in Puget Sound, Washington Sea Grant, Seattle.

Sutherland, D.A., P. MacCready, N.S. Banas and L.F. Smedstad, 2010, A Model Study of the Salish Sea Estuarine Circulation, submitted to Journal of Physical Oceanography.

Umlauf, L., and H. Burchard, 2003, A generic length-scale equation for geophysical turbulence, Journal of Marine Research, 61, 235-265.

Table 1

Statistical comparison of modeled and observed salinity at the Hoodsport ORCA buoy. Values are in PSU unless otherwise indicated.

	4 – 10m	11 – 50m	51 – 96m
Model mean	29.213	29.718	30.046
Observed mean	28.101	29.912	30.304
Model bias	+1.112	-0.194	-0.258
Model minimum/maximum/range	27.847 / 30.339 / 2.492	28.964 / 30.566 / 1.602	29.522 / 30.779 / 1.257
Observed minimum/maximum/range	24.188 / 29.930 / 5.742	29.029 / 30.807 / 1.778	29.834 / 30.934 / 1.100
Bias-corrected RMS model error / percentage of modeled range	0.791 / 31.7%	0.332 / 20.7%	0.280 / 22.2%

Table 2.
Statistical comparison of modeled and observed salinity at the Twanoh ORCA buoy. Values are in PSU unless otherwise indicated.

	3 – 10m	11m – Bottom
Model mean	28.097	29.506
Observed mean	27.334	29.622
Model bias	+0.763	-0.116
Model minimum/maximum/range	25.551 / 29.959/ 4.408	28.551 / 30.493 / 1.942
Observed minimum/maximum/range	22.419 / 29.375 / 6.956	28.085 / 30.738 / 2.653
Bias-corrected RMS model error / percentage of modeled range	1.017 / 23.1%	0.315/ 16.2%

Figure Captions

Figure 1. Map of Hood Canal, Washington showing locations of observations and the Oak Head section where transport is estimated.

Figure 2. Model grid. For clarity, only every other grid cell in each coordinate direction is shown. The actual grid has twice the resolution in each horizontal direction of the depicted.

Figure 3. (Top) Depth-averaged salinity boundary condition applied at the open boundary. Red circles indicate data taken from ADM001; green lines from Hansville ORCA. (Middle) River discharge used by the model from Steinberg et al. (200?). The total discharge as well as discharge from the five largest fresh water sources are plotted. Note the vertical axis is logarithmic. (Bottom) Hourly (gray) and low-passed (black) wind stress at Hoodsport ORCA (positive into the canal). Hourly wind is used for model forcing.

Figure 4. Low-passed modeled salinity (PSU) at the Hoodsport ORCA location over the model verification period.

Figure 5. Brunt-Väisälä frequency (radians per second) calculated from the low-passed modeled salinity at the Hoodsport ORCA location (Figure 4) for the model verification period.

Figure 6. Observed salinity (PSU) from Hoodsport ORCA over the model verification period.

Figure 7. Comparison of modeled (red) and observed (blue) low-passed salinity. (Top) Average over 4 – 10m. (Middle) Average over 11 – 50m. (Bottom) Average over 51 – 96m.

Figure 8. Observed temperature (°C) from from Hoodsport ORCA over the model verification period.

Figure 9. (Top) Low-passed modeled salinity (PSU) at the Twanoh ORCA location over the model verification period. (Bottom) Observed salinity (PSU) from Twanoh ORCA.

Figure 10. Comparison of modeled (red) and observed (blue) low-passed salinity at the Twanoh ORCA location. (Top) Average over 3 – 10m. (Bottom) Average over 11m to the bottom).

Figure 11. Comparison of modeled (red) and observed (blue) monthly average Brunt-Väisälä frequency for February, May, August and November of 2006.

Figure 12. Modeled low-passed along-channel current (m/s) at the Hoodsport ORCA location over the model verification period.

Figure 13. Low-passed along-channel current (m/s) observed from ADCP at the Hoodsport ORCA location over the model verification period.

Figure 14. Modeled average salinity (PSU) along the Hood Canal thalweg (color, PSU) and average overturning transport streamfunction Ψ (cubic meters per second, contour) for the entire model verification period. Entrance of the Canal is to the right. Heavy dashed line denotes the location of the Oak Head section (see Figure 1).

Figure 15. Bimonthly average salinity (PSU) and Ψ (cubic meters per second) as in Figure 14.

Figure 16. Low-passed daily salinity and Ψ as in Figure 14. (Top) June 19, 2006, a neap tide period; (Bottom) June 27, 2006, a spring tide period.

Figure 17. (Top) Salinity-averaged transport streamfunction Ψ_S (contour, cubic meters per second) and per-salinity transport $\partial\Psi_S/\partial S$ (color, positive into the Canal) as functions of salinity at the Oak Head section over the model verification period. (Bottom) Eulerian-averaged (blue) and salinity-averaged (green) transport of the exchange circulation at the Oak Head section, in comparison with the transport from the Babson et al. (2006) model (composite seasonal run). Horizontal dashed lines denote estimates of maximum and minimum transport at Hazel Point by Cokelet et al. (1990).

Figure 18. As in Figure 7, but for a run with an imposed temperature boundary condition at the open boundary from ADM001 and Hansville ORCA.

Figure 19. As in Figure 7, but with salinities from the no wind experiment (green), constant open boundary experiment (red), and constant river discharge experiment (blue) on top of the full forcing experiment (solid black) and observations (dashed black).

Figure 20. Eulerian-averaged transport at the Oak Head section, from the full forcing (black), no wind (green), constant open boundary (red), and constant river (blue) experiments.

Figure 1

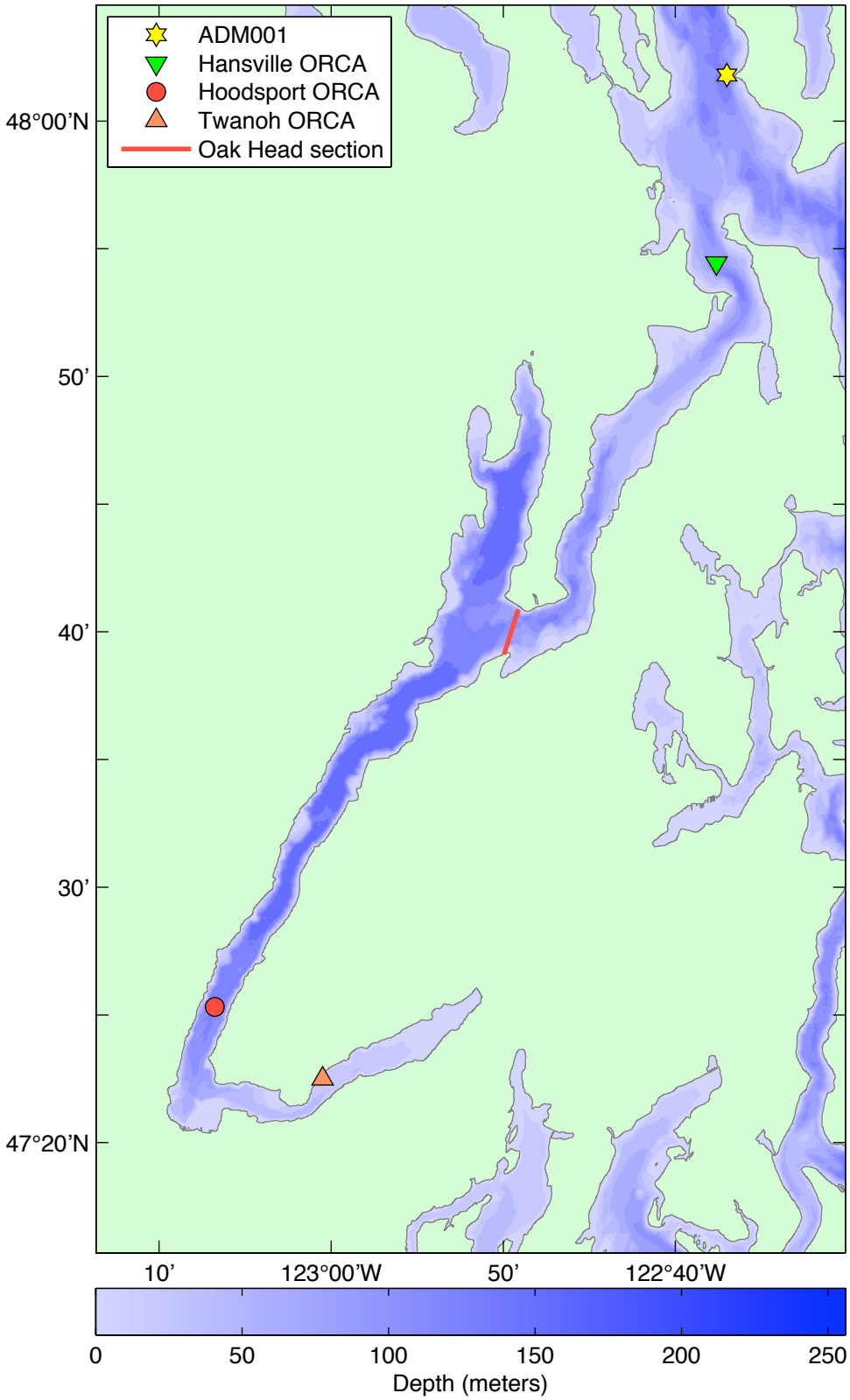
ADM001
Hansville ORCA
Hoodsport ORCA
Twanoh ORCA
Oak Head section
48°00'N
50'
40'
30'
47°20'N
10'
123°00'W
50'
122°40'W
0
50
100
150
200
250
Depth (meters)

Figure 2

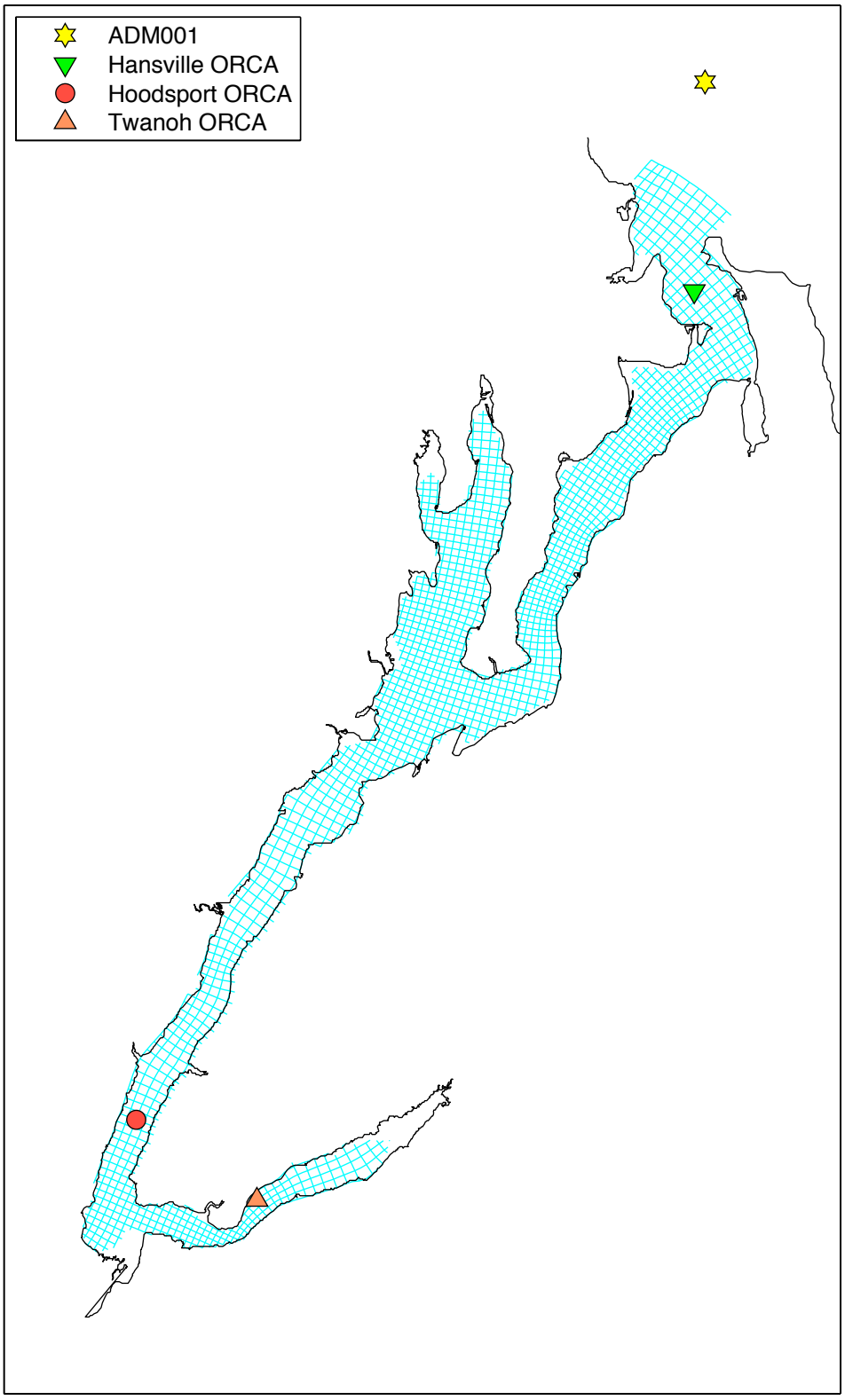

Figure 3

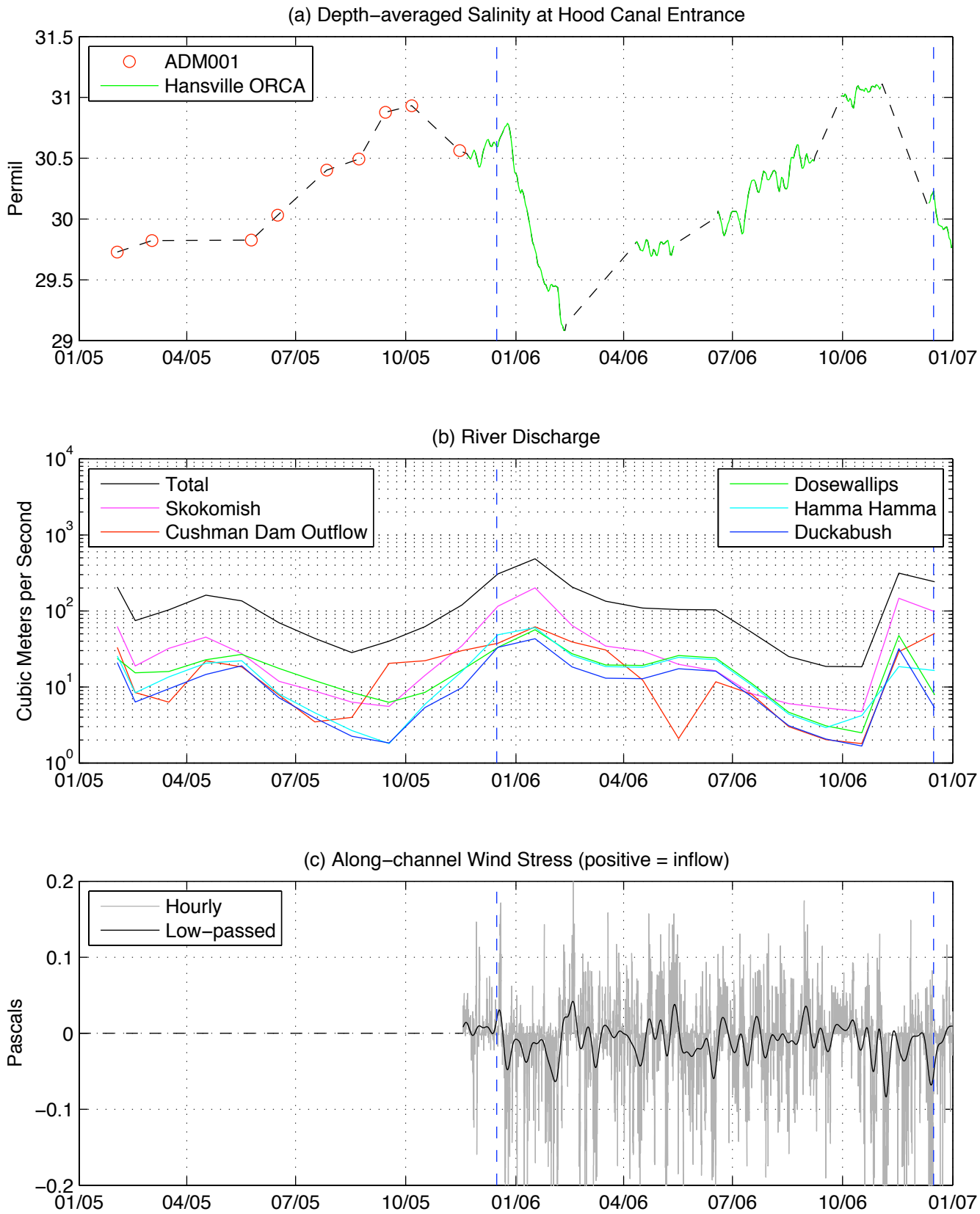
(a) Depth−averaged Salinity at Hood Canal Entrance
ADM001
Hansville ORCA
Permil
31.5
31
30.5
30
29.5
29
01/05
04/05
07/05
10/05
01/06
04/06
07/06
10/06
01/07
(b) River Discharge
Total
Skokomish
Cushman Dam Outflow
Dosewallips
Hamma Hamma
Duckabush
Cubic Meters per Second
10^4
10^3
10^2
10^1
10^0
(c) Along−channel Wind Stress (positive = inflow)
Hourly
Low−passed
Pascals
0.2
0.1
0
−0.1
−0.2

Figure 4

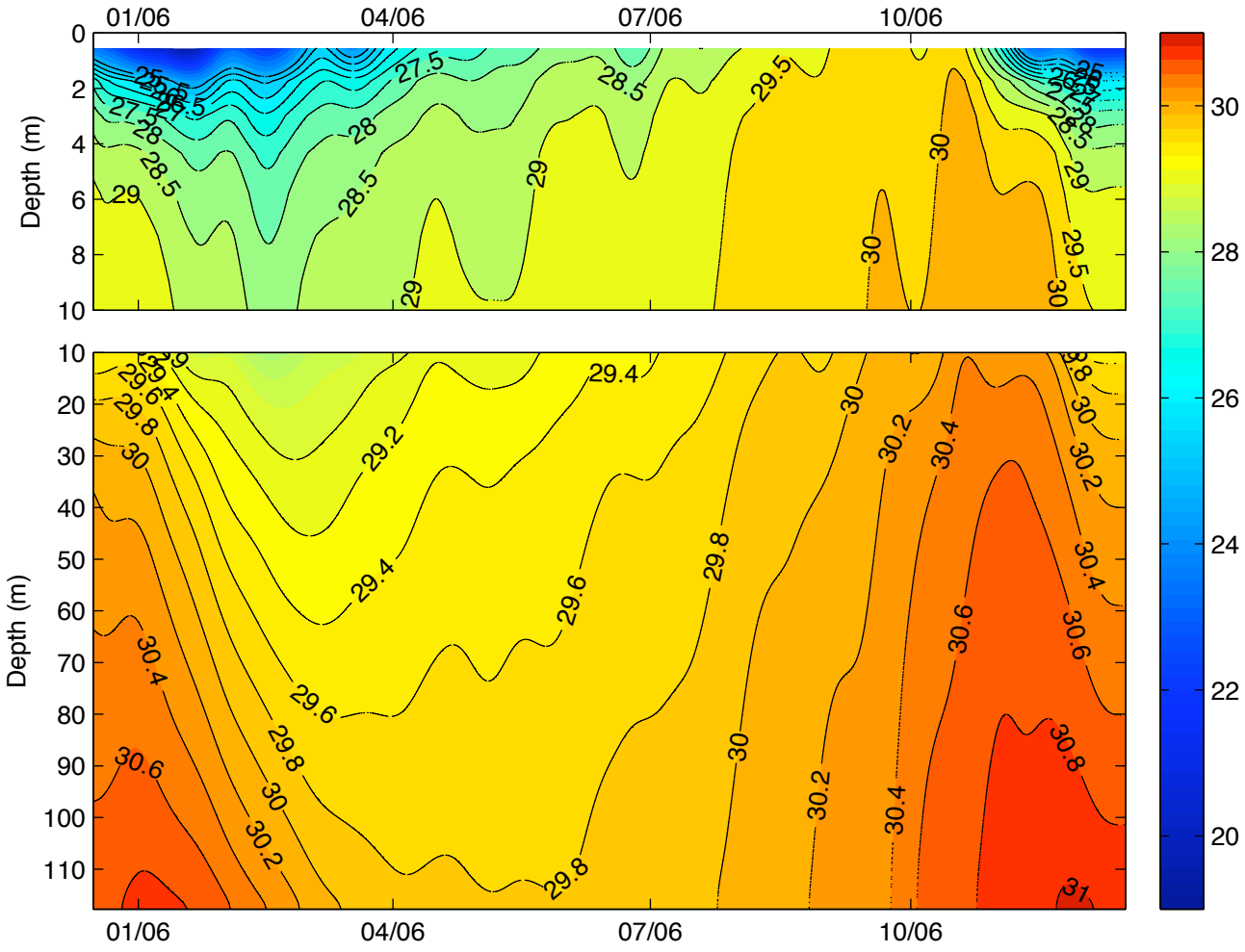
01/06
04/06
07/06
10/06
Depth (m)
0
2
4
6
8
10
10
20
30
40
50
60
70
80
90
100
110
20
22
24
26
28
30

Figure 5

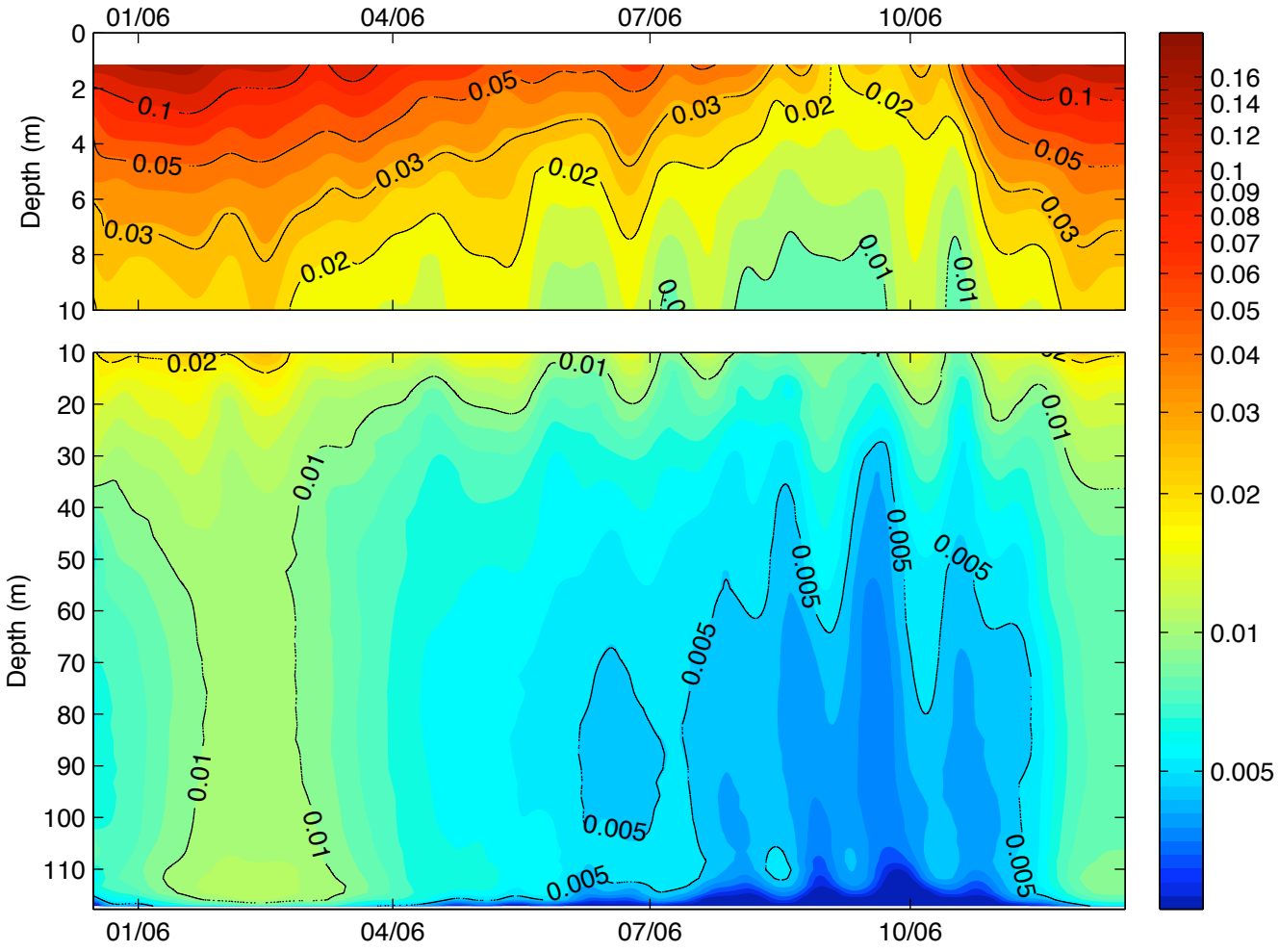
01/06
04/06
07/06
10/06
Depth (m)
0
2
4
6
8
10
0.1
0.05
0.03
0.02
0.01
10
20
30
40
50
60
70
80
90
100
110
0.16
0.14
0.12
0.1
0.09
0.08
0.07
0.06
0.05
0.04
0.03
0.02
0.01
0.005

Figure 6

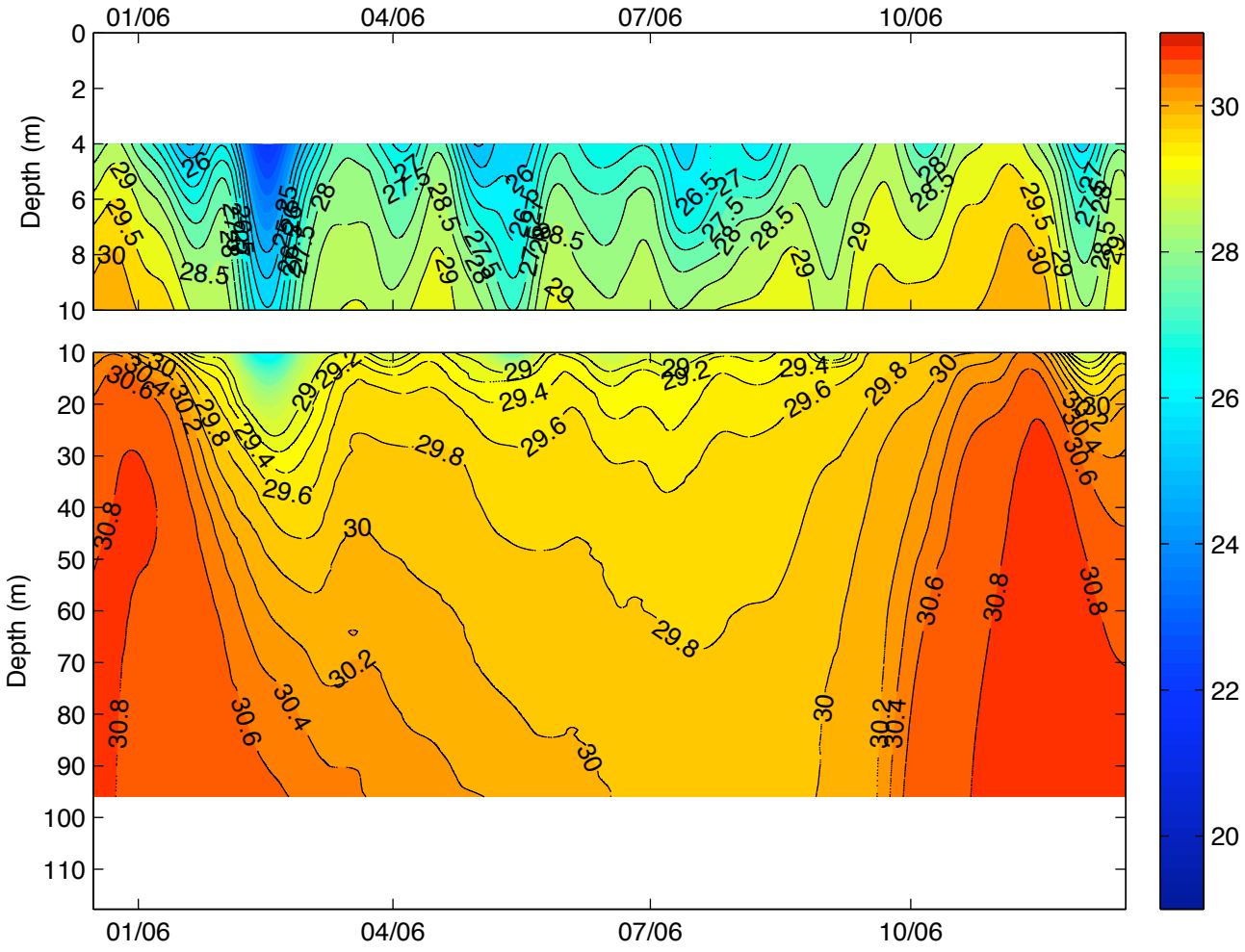
01/06
04/06
07/06
10/06
Depth (m)
0
2
4
6
8
10
10
20
30
40
50
60
70
80
90
100
110
30
28
26
24
22
20

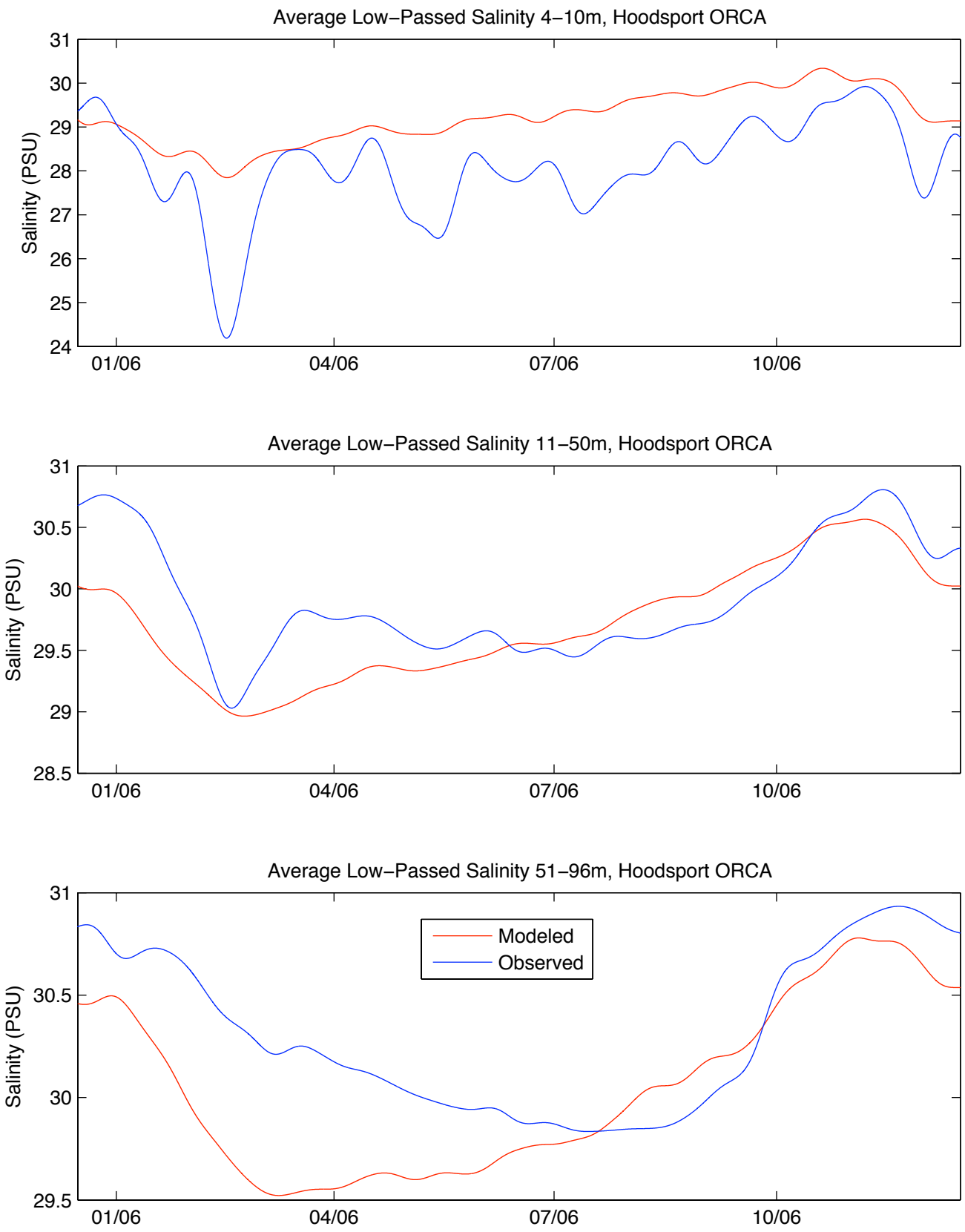
Average Low−Passed Salinity 4−10m, Hoodsport ORCA
Salinity (PSU)
31
30
29
28
27
26
25
24
01/06
04/06
07/06
10/06
Average Low−Passed Salinity 11−50m, Hoodsport ORCA
Salinity (PSU)
31
30.5
30
29.5
29
28.5
01/06
04/06
07/06
10/06
Average Low−Passed Salinity 51−96m, Hoodsport ORCA
Salinity (PSU)
31
30.5
30
29.5
Modeled
Observed
01/06
04/06
07/06
10/06

Figure 8

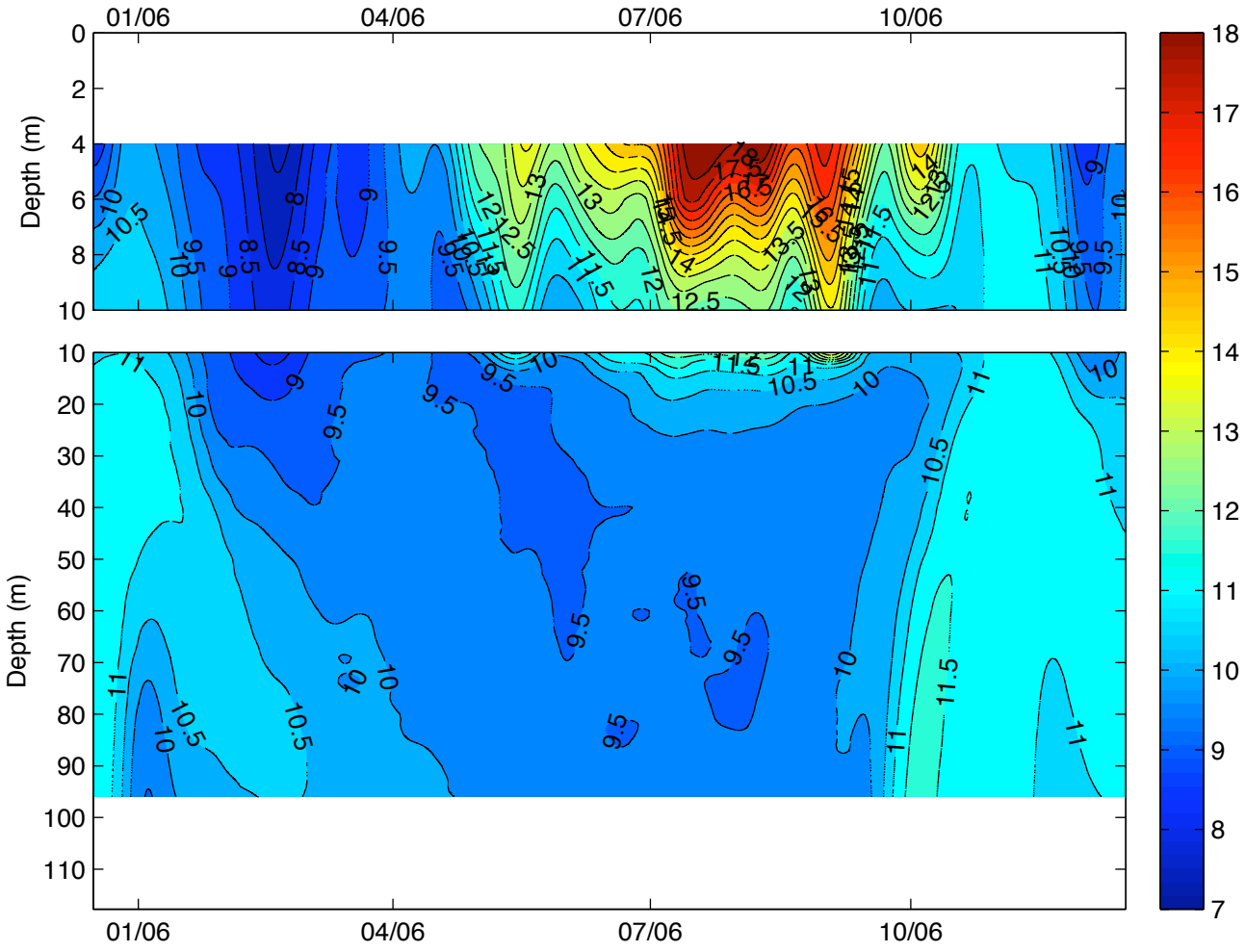
01/06
04/06
07/06
10/06
Depth (m)
0
2
4
6
8
10
10
20
30
40
50
60
70
80
90
100
110
18
17
16
15
14
13
12
11
10
9
8
7

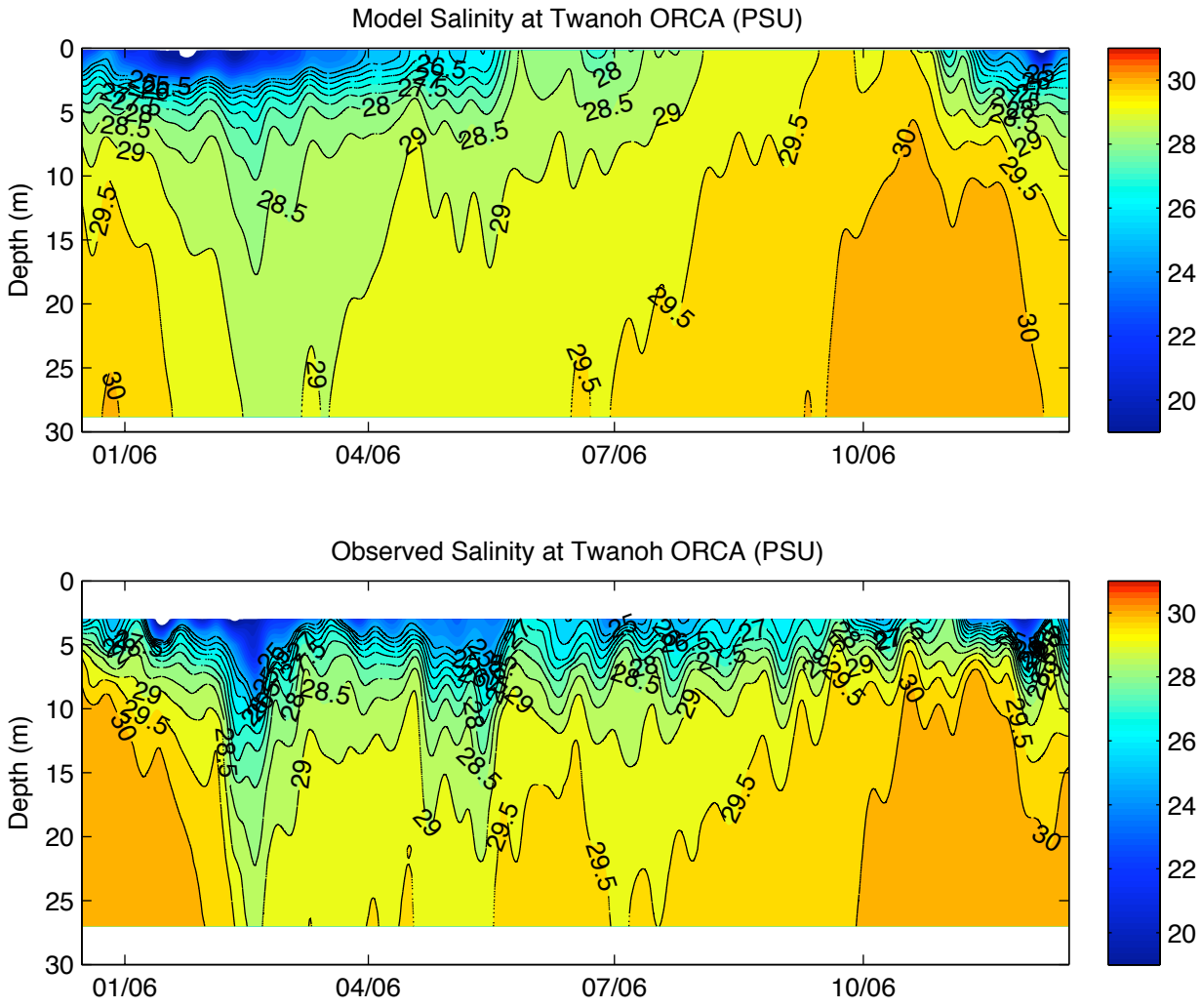
Model Salinity at Twanoh ORCA (PSU)
Depth (m)
0
5
10
15
20
25
30
01/06
04/06
07/06
10/06
20
22
24
26
28
30
Observed Salinity at Twanoh ORCA (PSU)
Depth (m)
01/06
04/06
07/06
10/06

Figure 10

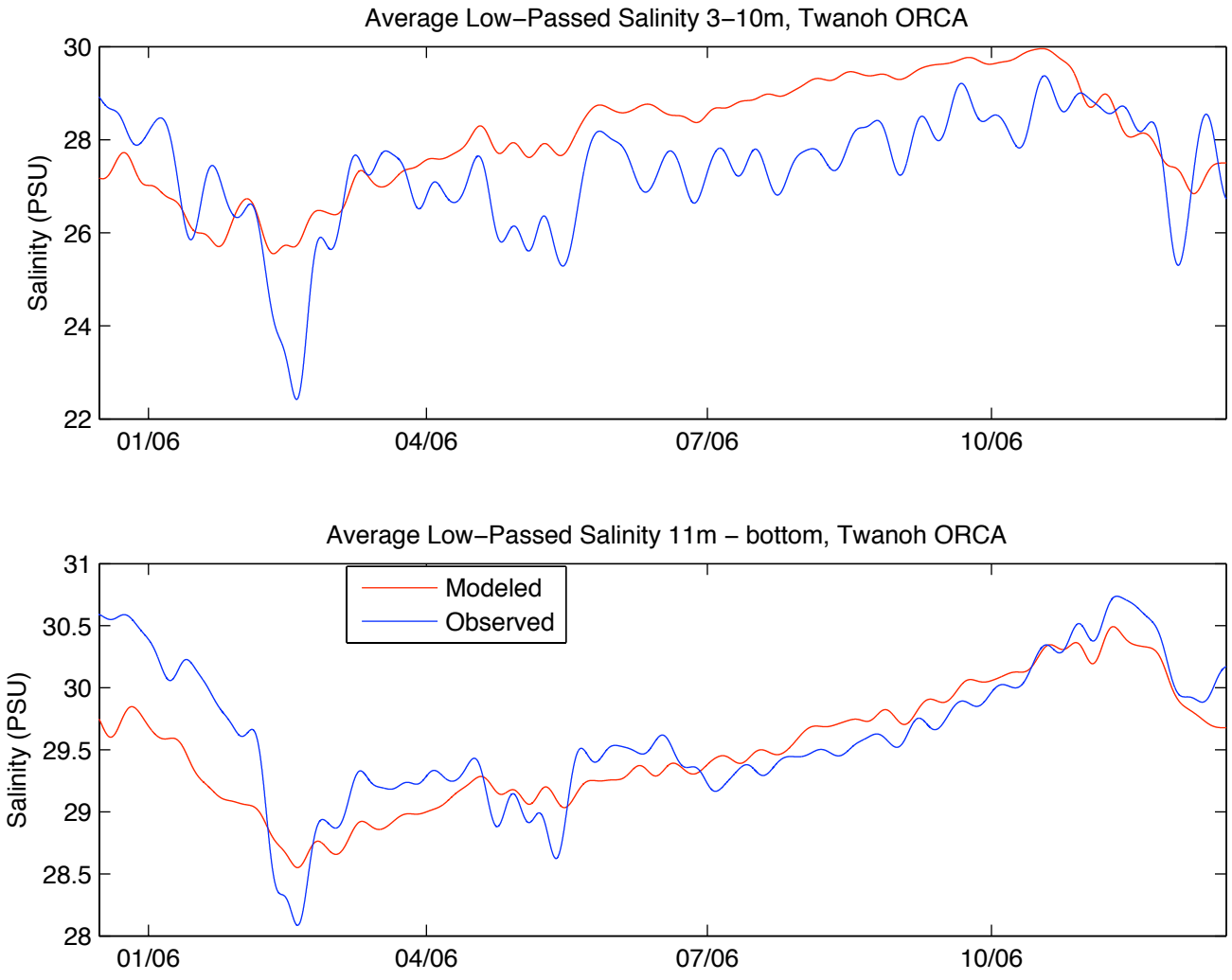
Average Low−Passed Salinity 3−10m, Twanoh ORCA
Salinity (PSU)
30
28
26
24
22
01/06
04/06
07/06
10/06
Average Low−Passed Salinity 11m − bottom, Twanoh ORCA
Modeled
Observed
Salinity (PSU)
31
30.5
30
29.5
29
28.5
28
01/06
04/06
07/06
10/06

Figure 11

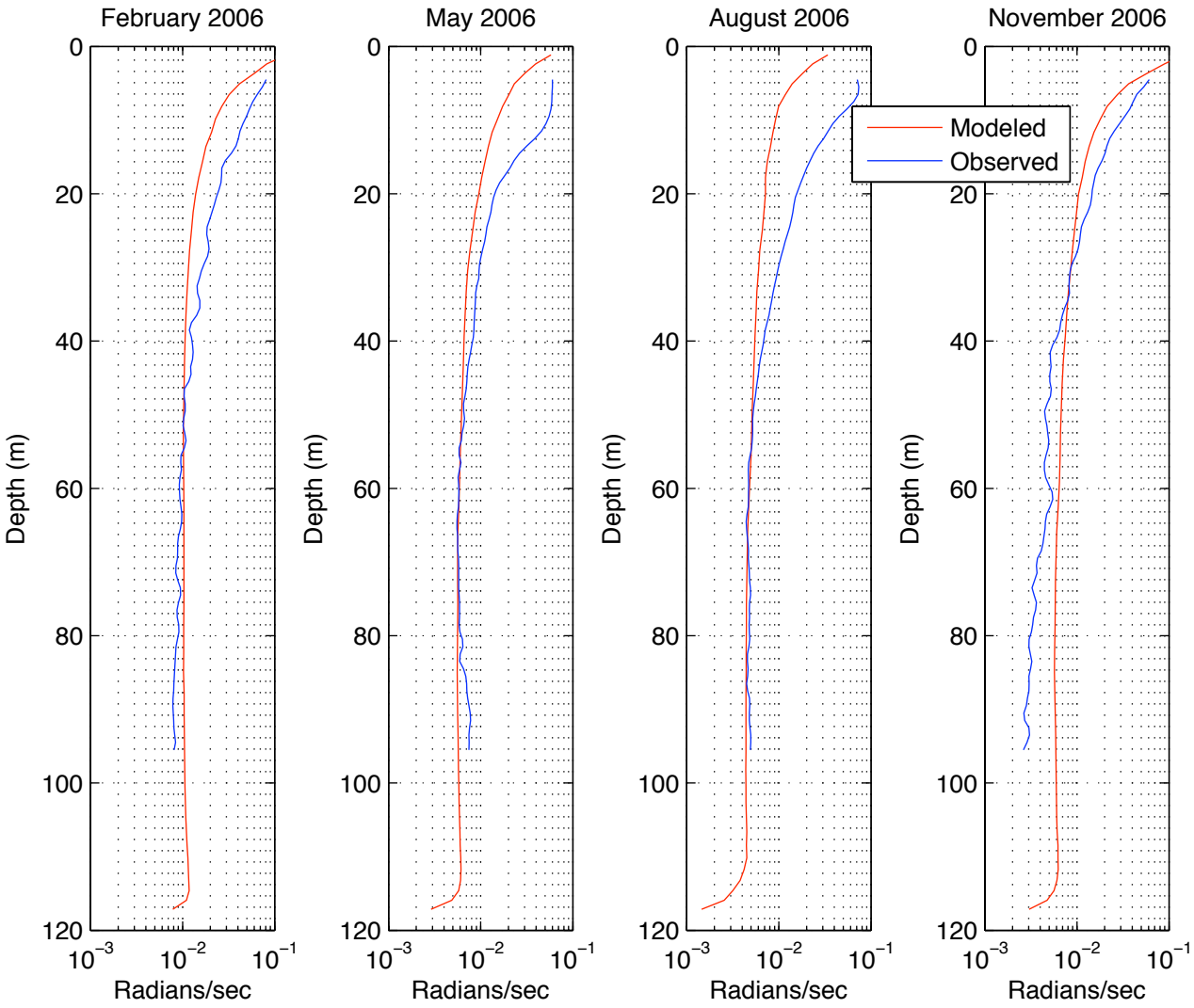
February 2006
May 2006
August 2006
November 2006
Depth (m)
0
20
40
60
80
100
120
10^{-3}
10^{-2}
10^{-1}
Radians/sec
Modeled
Observed

Figure 12

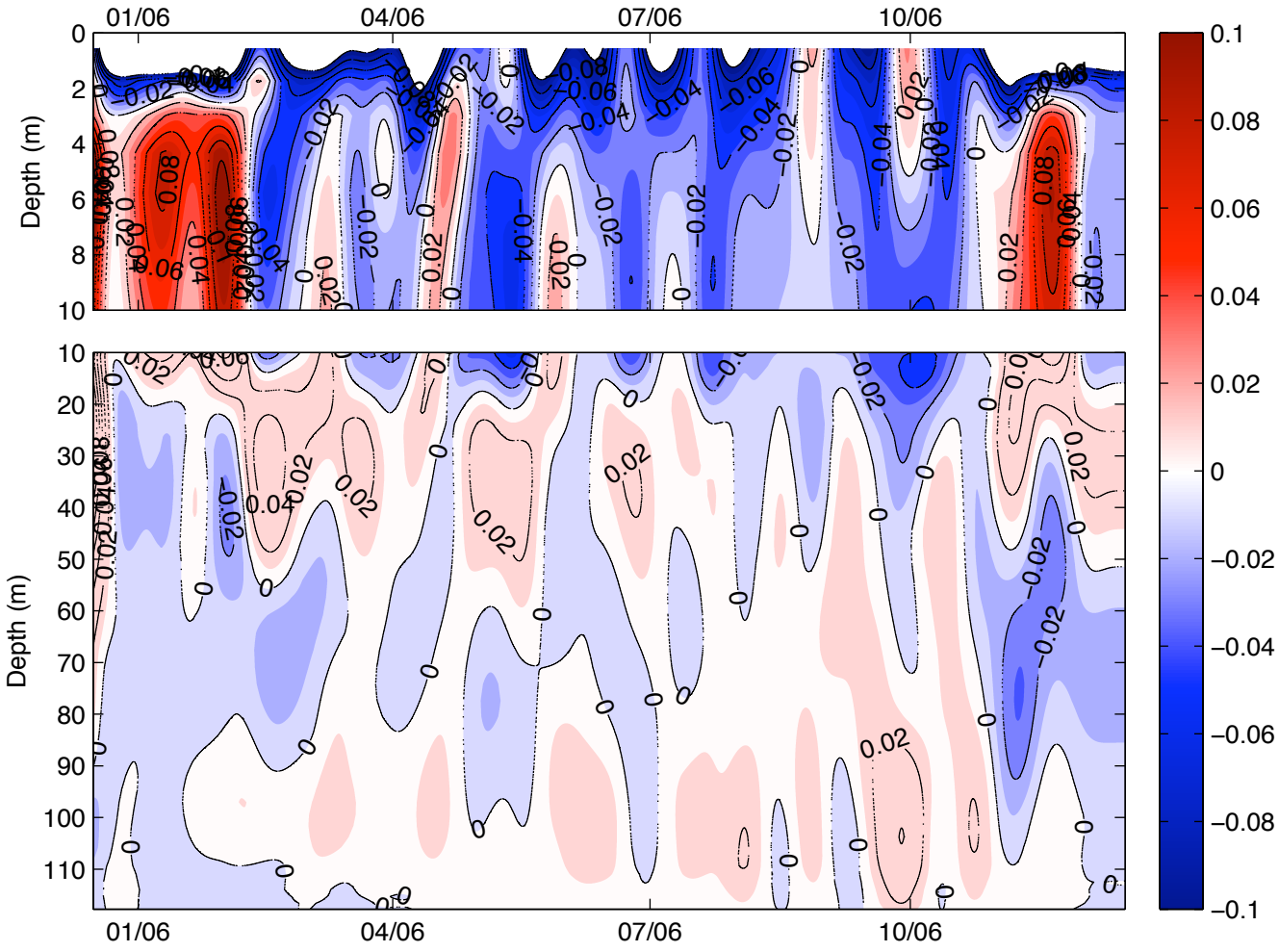
01/06
04/06
07/06
10/06
Depth (m)
0
2
4
6
8
10
10
20
30
40
50
60
70
80
90
100
110
0.1
0.08
0.06
0.04
0.02
0
−0.02
−0.04
−0.06
−0.08
−0.1

Figure 13

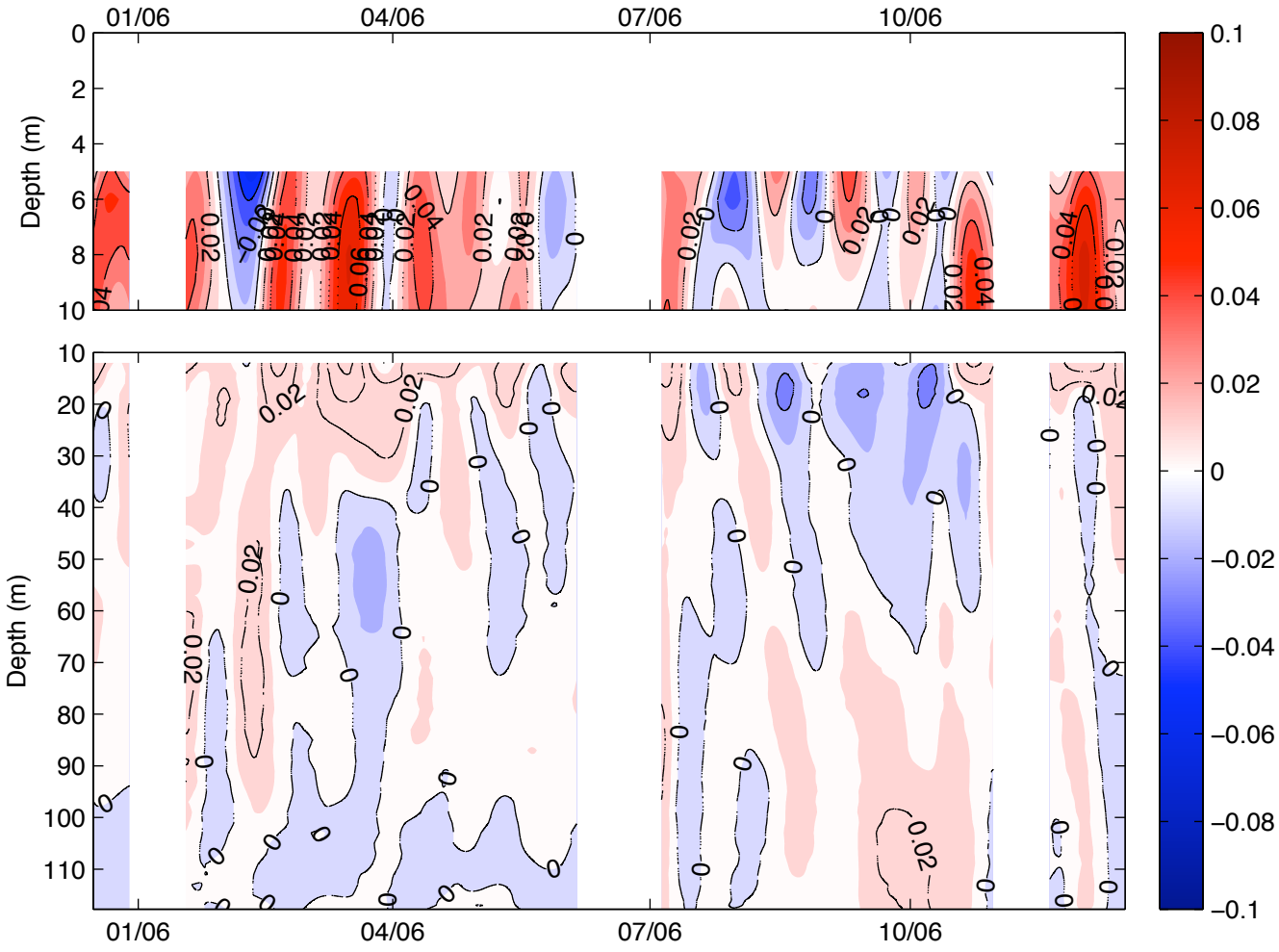
01/06
04/06
07/06
10/06
Depth (m)
0
2
4
6
8
10
10
20
30
40
50
60
70
80
90
100
110
0.1
0.08
0.06
0.04
0.02
0
−0.02
−0.04
−0.06
−0.08
−0.1

Figure 14

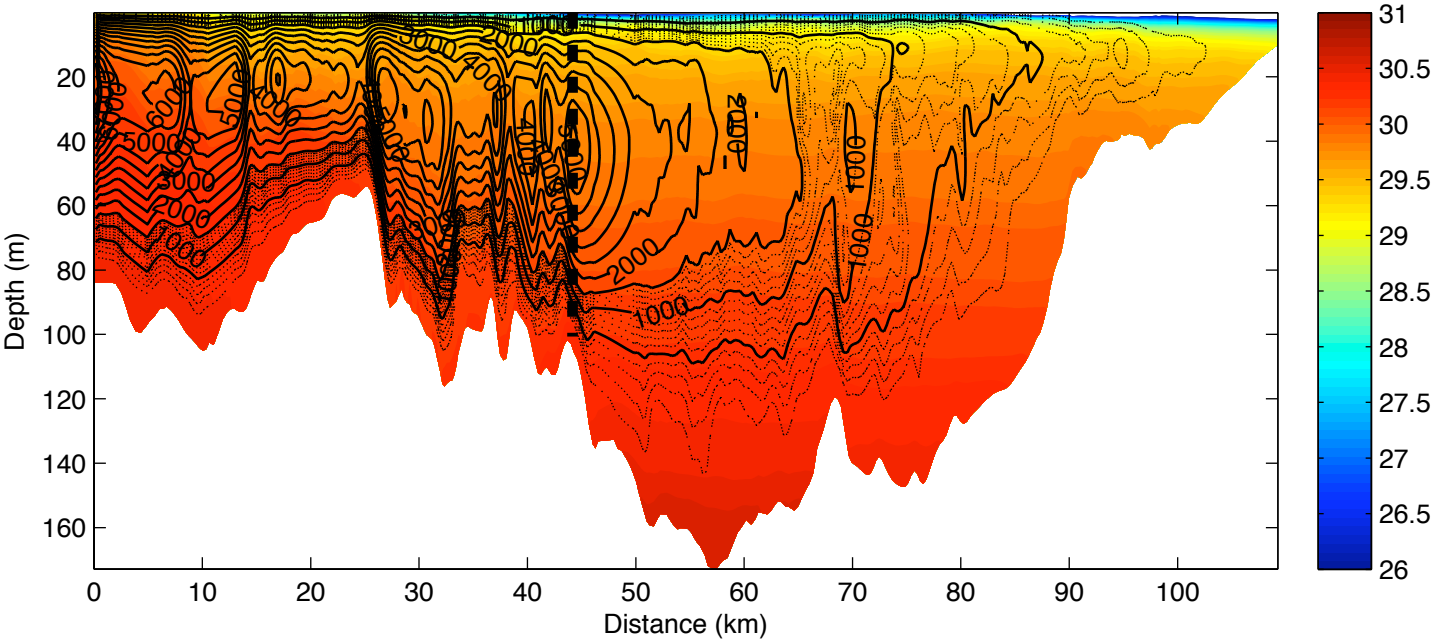
Depth (m)
20
40
60
80
100
120
140
160
0
10
20
30
40
50
60
70
80
90
100
Distance (km)
31
30.5
30
29.5
29
28.5
28
27.5
27
26.5
26

Figure 15

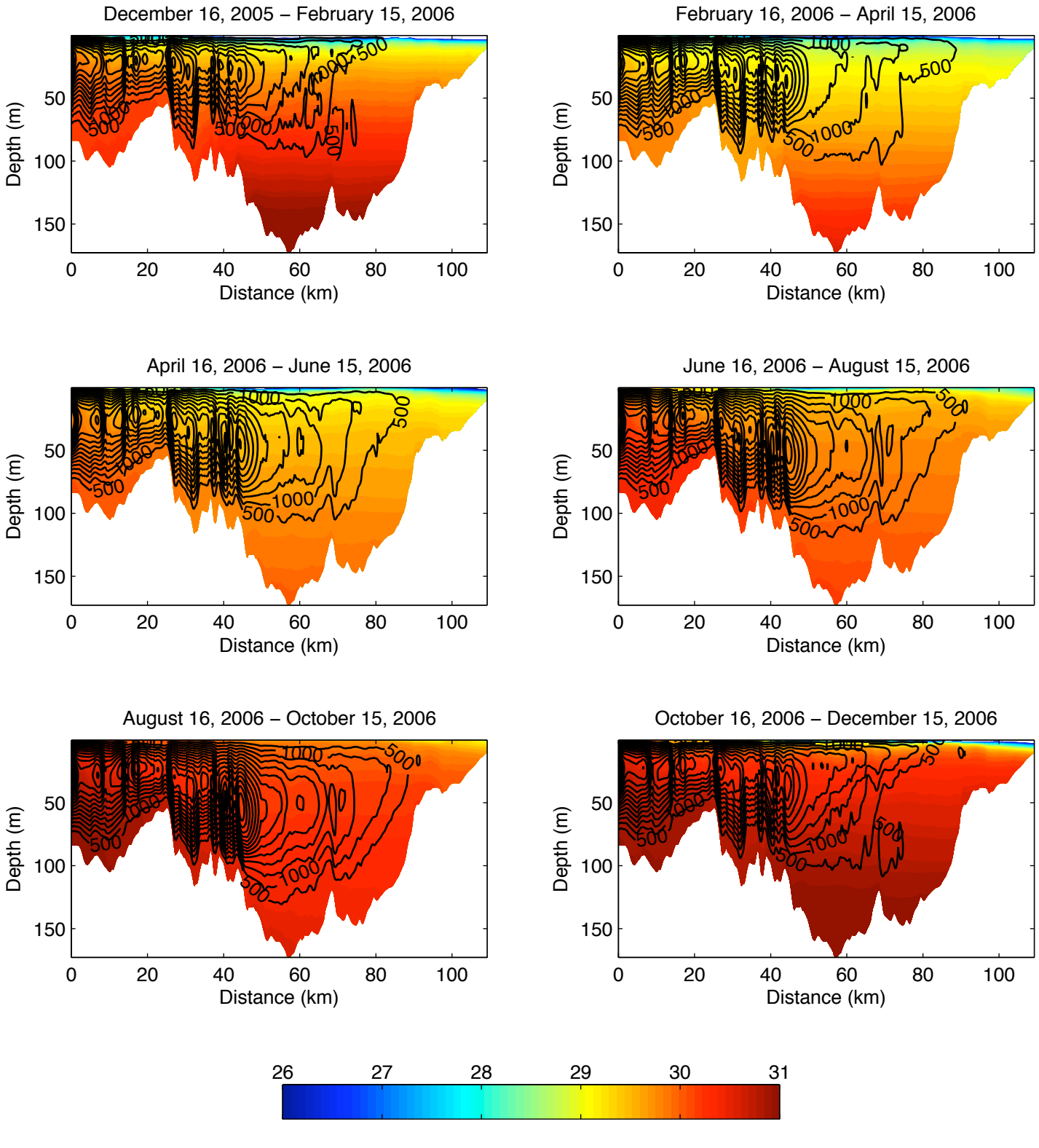
December 16, 2005 – February 15, 2006
February 16, 2006 – April 15, 2006
April 16, 2006 – June 15, 2006
June 16, 2006 – August 15, 2006
August 16, 2006 – October 15, 2006
October 16, 2006 – December 15, 2006
Depth (m)
Distance (km)
0
20
40
60
80
100
50
100
150
26
27
28
29
30
31

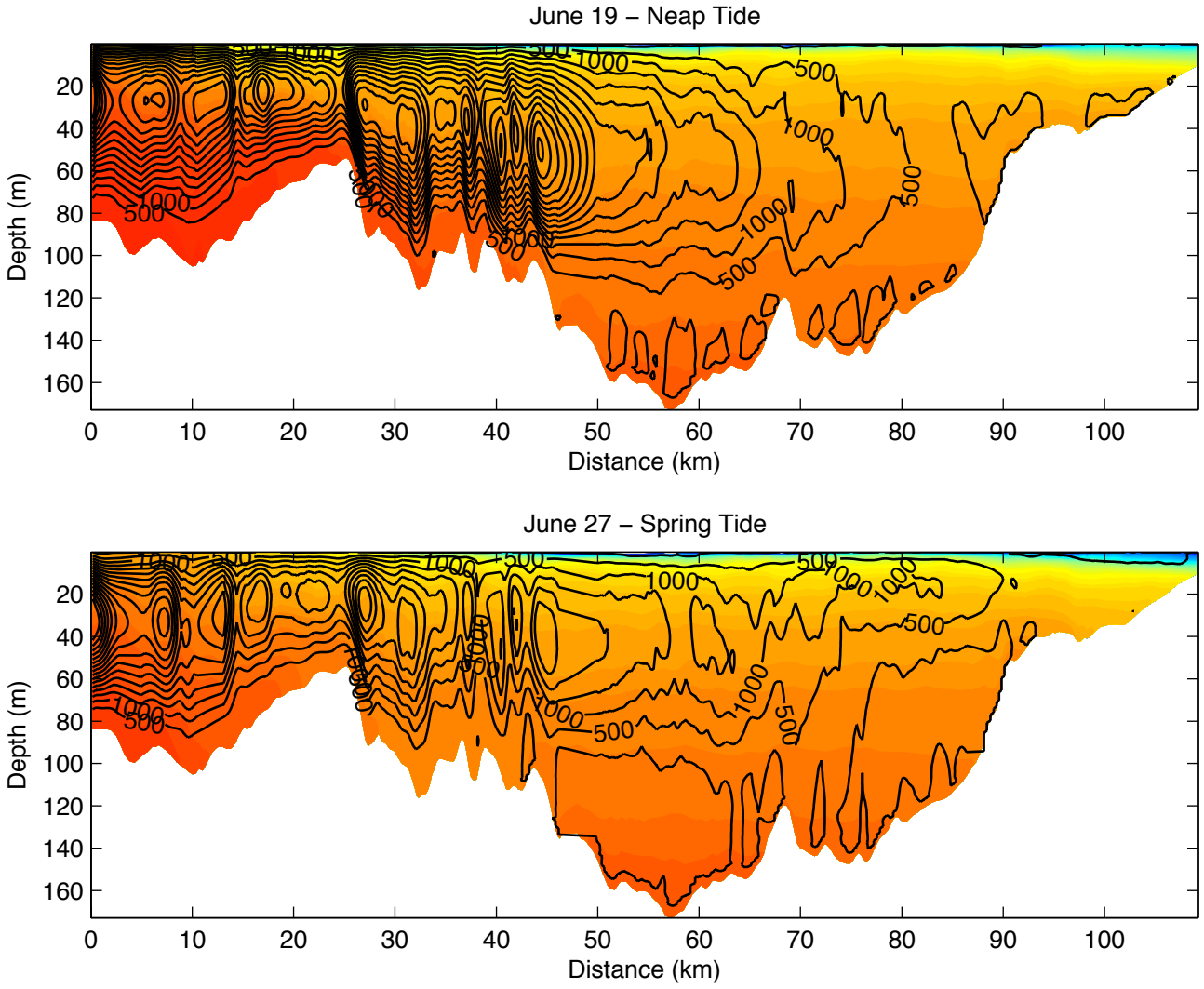
June 19 – Neap Tide
Depth (m)
Distance (km)
June 27 – Spring Tide
Depth (m)
Distance (km)

Figure 17

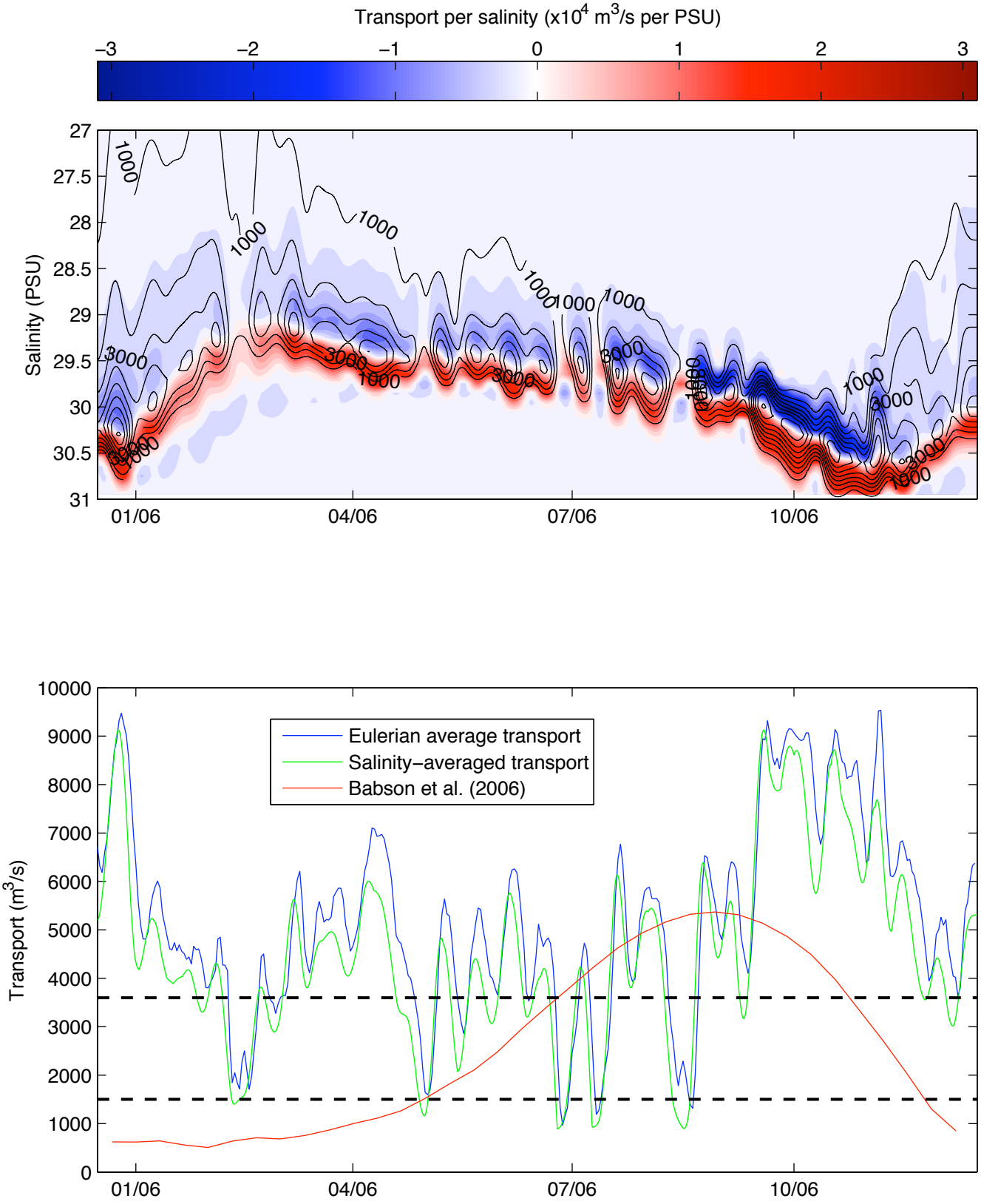
Transport per salinity (x10^4 m^3/s per PSU)
−3
−2
−1
0
1
2
3
Salinity (PSU)
27
27.5
28
28.5
29
29.5
30
30.5
31
1000
3000
01/06
04/06
07/06
10/06
Transport (m^3/s)
10000
9000
8000
7000
6000
5000
4000
3000
2000
1000
0
Eulerian average transport
Salinity−averaged transport
Babson et al. (2006)

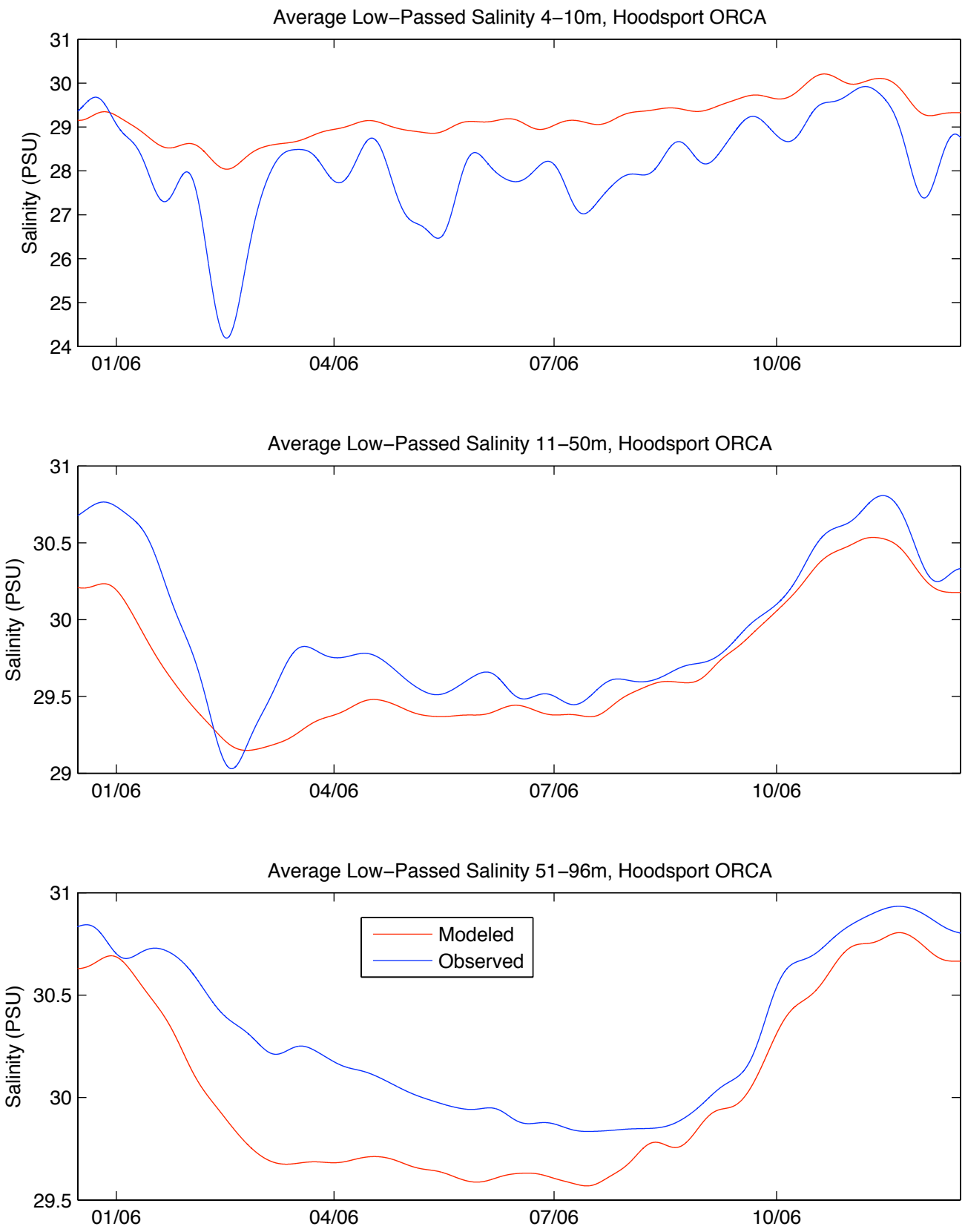
Average Low−Passed Salinity 4−10m, Hoodsport ORCA
Salinity (PSU)
31
30
29
28
27
26
25
24
01/06
04/06
07/06
10/06
Average Low−Passed Salinity 11−50m, Hoodsport ORCA
Salinity (PSU)
31
30.5
30
29.5
29
01/06
04/06
07/06
10/06
Average Low−Passed Salinity 51−96m, Hoodsport ORCA
Modeled
Observed
Salinity (PSU)
31
30.5
30
29.5
01/06
04/06
07/06
10/06

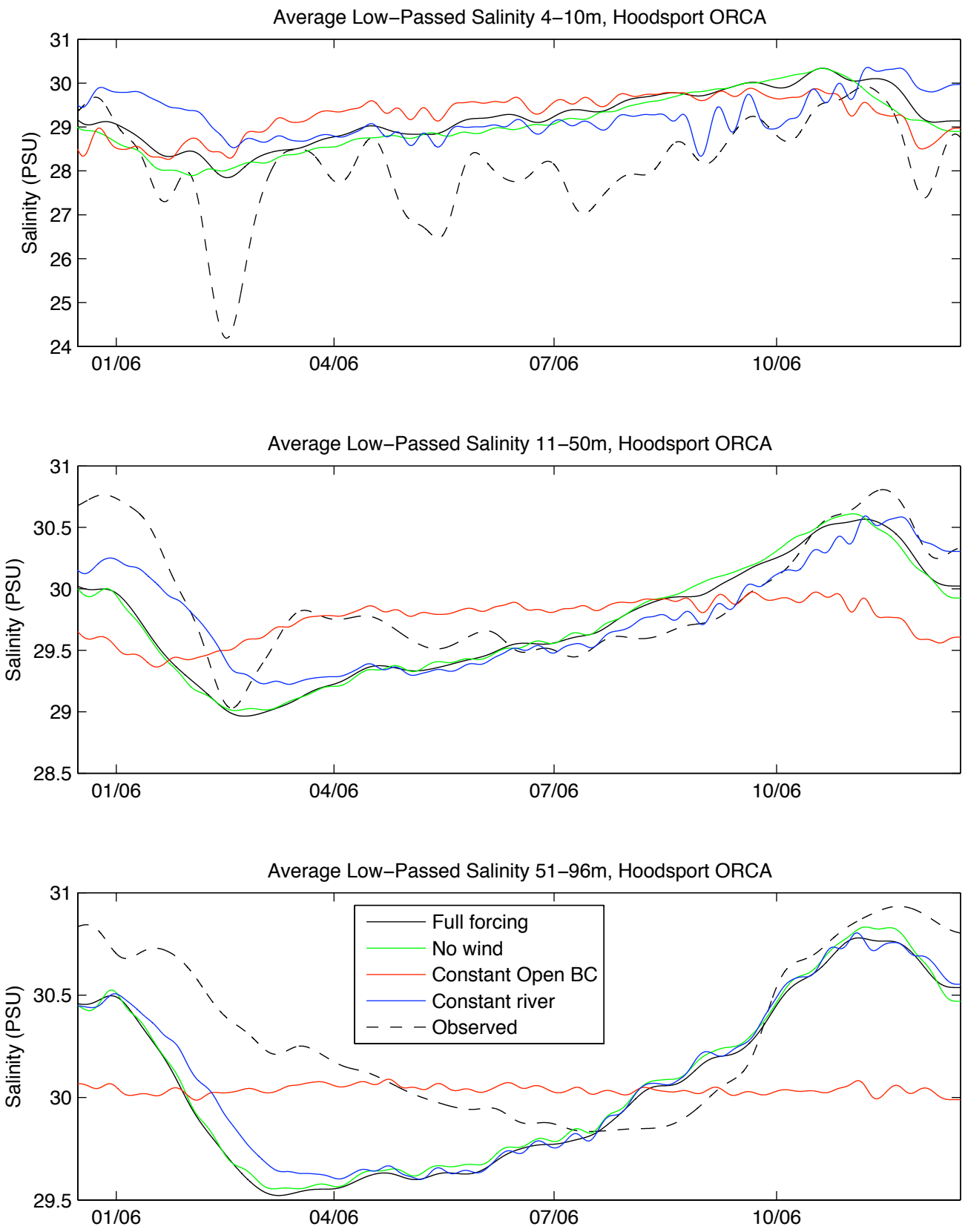
Average Low−Passed Salinity 4−10m, Hoodsport ORCA
Salinity (PSU)
31
30
29
28
27
26
25
24
01/06
04/06
07/06
10/06
Average Low−Passed Salinity 11−50m, Hoodsport ORCA
Salinity (PSU)
31
30.5
30
29.5
29
28.5
01/06
04/06
07/06
10/06
Average Low−Passed Salinity 51−96m, Hoodsport ORCA
Salinity (PSU)
31
30.5
30
29.5
01/06
04/06
07/06
10/06
Full forcing
No wind
Constant Open BC
Constant river
Observed

Figure 20

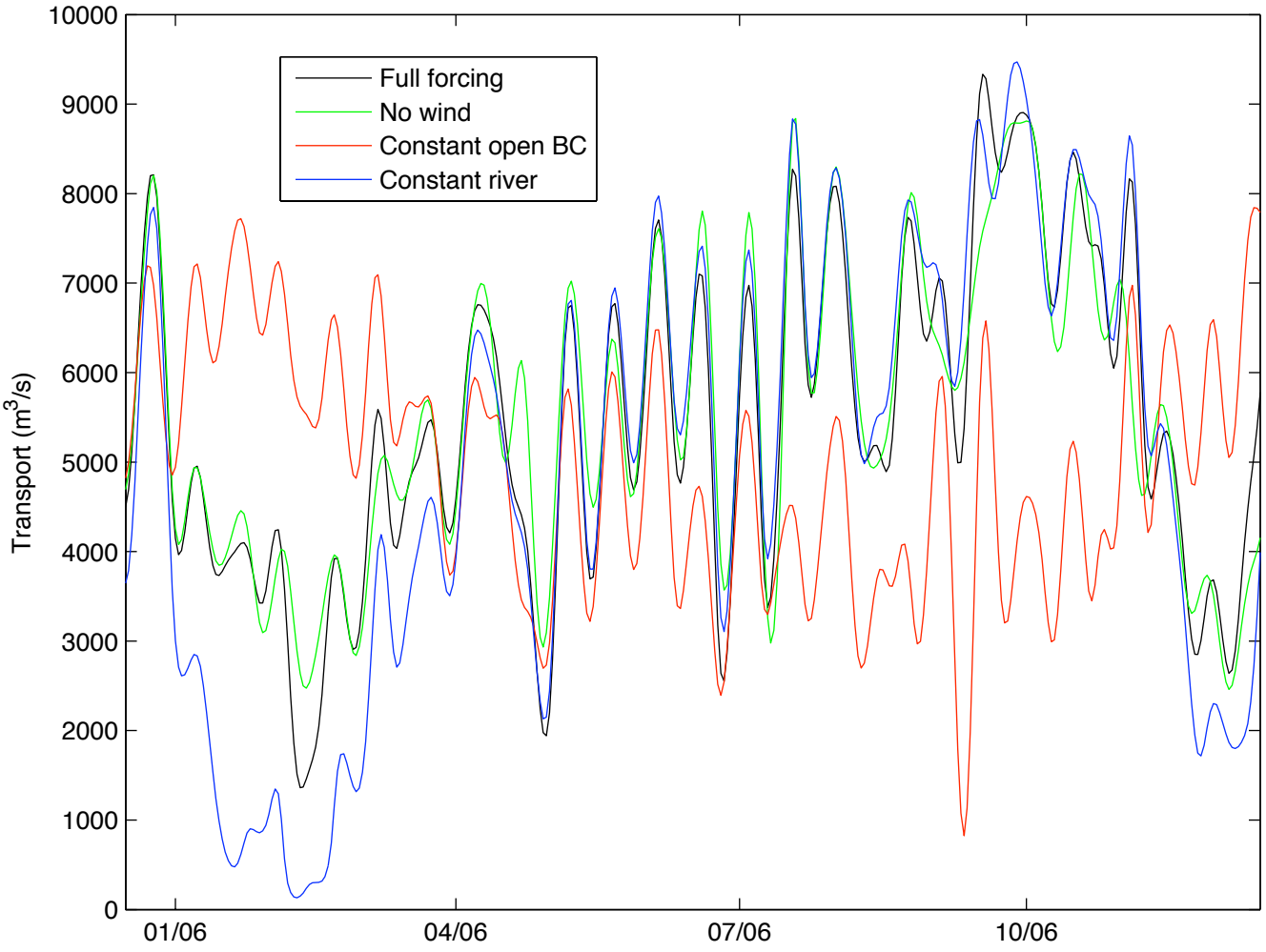
Full forcing
No wind
Constant open BC
Constant river
Transport (m3/s)
10000
9000
8000
7000
6000
5000
4000
3000
2000
1000
0
01/06
04/06
07/06
10/06